

BIOPHYSICS

Characterization of the membrane interactions of phospholipase C γ reveals key features of the active enzyme

Kyle I. P. Le Huray^{1,2,3}, Tom D. Bunney^{4*}, Nikos Pinotsis⁵, Antreas C. Kalli^{1,3*}, Matilda Katan^{4*}

PLC γ enzymes are autoinhibited in resting cells and form key components of intracellular signaling that are also linked to disease development. Insights into physiological and aberrant activation of PLC γ require understanding of an active, membrane-bound form, which can hydrolyze inositol-lipid substrates. Here, we demonstrate that PLC γ 1 cannot bind membranes unless the autoinhibition is disrupted. Through extensive molecular dynamics simulations and experimental evidence, we characterize membrane binding by the catalytic core domains and reveal previously unknown sites of lipid interaction. The identified sites act in synergy, overlap with autoinhibitory interfaces, and are shown to be critical for the phospholipase activity in cells. This work provides direct evidence that PLC γ 1 is inhibited through obstruction of its membrane-binding surfaces by the regulatory region and that activation must shift PLC γ 1 to a conformation competent for membrane binding. Knowledge of the critical sites of membrane interaction extends the mechanistic framework for activation, dysregulation, and therapeutic intervention.

INTRODUCTION

Receptors for a wide range of external stimuli, such as neurotransmitters, agonists for immune cell receptors, hormones, and growth factors, activate core signaling modules, including phospholipase C (PLC) enzymes (1). PLC enzymes catalyze the hydrolysis of inositol lipids, mainly phosphatidylinositol 4,5-bisphosphate (PIP₂) to second messengers inositol 1,4,5-trisphosphate (IP₃) and diacylglycerol. In addition, PLC enzymes can affect the function of a range of PIP₂-binding proteins by changing local concentrations of PIP₂ (2). Numerous studies of individual PLCs, including the 16 isoforms in humans, revealed a rich repertoire of PLC functions in different physiological contexts. Furthermore, genetic studies have uncovered many mutated and rare variants of PLC enzymes, particularly in the PLC γ family, and their link to human disease development (1, 3). Specifically, variants of PLC γ 1 and PLC γ 2 have been linked to cancer, complex immune disorders, inflammation (further implicated in other diseases), and Alzheimer's and related neurodegenerative diseases [see (4–11) for the major, comprehensive discoveries].

The understanding of the molecular mechanisms of regulation and dysregulation of PLC enzymes has been facilitated by studies of individual isoforms and their complexes with regulatory proteins (12–20). An emerging general concept of PLC activation is centered on intramolecular interactions that maintain PLCs in their inactive form, also referred to as autoinhibition, that becomes released in the process of activation in stimulated cells. All structures reported so far seem to represent autoinhibited forms of PLCs. Nevertheless, it is clear that an active form of PLC enzymes must interact with the membrane for the efficient binding and hydrolysis of inositol lipid

substrates. The catalytic activity in all PLCs is encapsulated within the TIM (triose-phosphate isomerase) barrel fold structure, which, in most isoforms, together with a PH domain, C2 domain, and EF hands, forms a common PLC core (1).

Comprehensive analyses of some of the PLC enzymes also identified specific features involved in regulation of a particular family and suggested that membrane interactions could be quite complex, with multiple roles. In this respect, members of the PLC β family have been studied most extensively; in addition to structural studies (13–17), regulation of these enzymes has been analyzed in the presence of different model membranes *in vitro* (21–25). In its basal state, PLC β is autoinhibited by the XY-linker from the catalytic TIM barrel and by elements from the C-terminal domain, representing a unique feature of PLC β enzymes. Activation of PLC β involves allosteric conformational changes resulting from the binding of G α q or G β γ subunits of heterotrimeric G proteins. PLC β interactions with the membrane are also likely to contribute to displacement of autoinhibitory constraints, resulting in interfacial activation.

Compared to PLC β , insights that revealed autoinhibitory interactions in the PLC γ family have been obtained relatively recently from structures of PLC γ 1 (18, 19). PLC γ enzymes are characterized by an array of domains, referred to as “ γ -specific array (γ SA)” or as “regulatory region,” encompassing the sPH, nSH2, cSH2, and SH3 domains. The autoinhibitory interfaces lock the γ SA on top of the PLC core. The structures also suggest mechanisms of activation via physiologically relevant phosphorylation of PLC γ by tyrosine kinases and by gain-of-function mutations discovered across diverse pathologies. The location of mutated amino acids mapped to the structure of PLC γ 1 reveals that many, including most of the hotspot alterations, are likely to directly release autoinhibition (18, 19). With respect to the PLC core, it has been established that although the same domains (nPH, EF-hand, catalytic TIM barrel, and C2 domains) are present in other families, their function varies, except for the catalytic domain (1). Despite initial studies suggesting the role of the PLC γ 1 nPH domain in selective binding of PI (3,4,5)P₃ and the involvement of PLC γ 2 C2 domain in Ca²⁺-dependent translocation to the membrane, the overall, direct information about membrane interactions and their

Copyright © 2022
The Authors, some
rights reserved;
exclusive licensee
American Association
for the Advancement
of Science. No claim to
original U.S. Government
Works. Distributed
under a Creative
Commons Attribution
License 4.0 (CC BY).

¹Astbury Centre for Structural Molecular Biology, Faculty of Biological Sciences, University of Leeds, Leeds LS2 9JT, UK. ²School of Molecular and Cellular Biology, Faculty of Biological Sciences, University of Leeds, Leeds, LS2 9JT UK. ³Leeds Institute of Cardiovascular and Metabolic Medicine, School of Medicine, University of Leeds, Leeds LS2 9JT, UK. ⁴Institute of Structural and Molecular Biology, Division of Biosciences, University College London, Gower St., London WC1E 6BT, UK. ⁵Institute of Structural and Molecular Biology, Birkbeck College, London, WC1E 6BT, UK. *Corresponding author. Email: t.bunney@ucl.ac.uk (T.D.B); a.kalli@leeds.ac.uk (A.C.K.); m.katan@ucl.ac.uk (M.K.)

possible roles are lacking for PLC γ enzymes (26, 27). Furthermore, as is the case for other PLCs, the active form of PLC γ has not been structurally defined, and this will be required to understand fully the activation processes and different mechanistic classes of disease-linked mutations.

Insights into an active form of PLC enzymes, including PLC γ , are closely linked to understanding of protein/membrane interactions, which bring the enzymes to the membrane proximity, and interactions that position the TIM barrel domain in a productive orientation for catalysis. On the basis of the current evidence, it is likely that an active form can be captured for structural studies only in the presence of model membranes that could be required to stabilize this form or, in some instances, to generate an active form through a membrane-dependent process. These types of protein/membrane complexes still present a challenge for most current structural approaches. Molecular dynamics (MD simulations) can fill this gap, by providing realistic insights into the interactions of proteins with model membranes (28–30). In particular, MD simulations have been used to predict membrane-binding interfaces, identify lipid binding sites and membrane-inserting regions for key signaling proteins including PTEN, KRAS, bacterial phospholipases, and pleckstrin homology domains (31–35).

In this study, we used these computational methods to examine the membrane interactions of PLC γ 1, in combination with crystallography, direct assessments of protein binding to liposomes, and measurements of PLC activity *in vitro* and in cells. We identified surfaces and key residues involved in extensive interactions with anionic lipids, especially phosphoinositides, and those inserted into the hydrophobic membrane core. We have also shown the importance of a number of these key residues for overall membrane binding, productive substrate recognition, and catalysis. Furthermore, we found that the regions involved in membrane binding largely overlap with autoinhibitory interfaces on the PLC core. These findings, which identify previously unknown features of membrane interactions of an active enzyme, shed new light on regulation of PLC γ enzymes.

RESULTS

Structure of autoinhibited PLC γ 1 in complex with IP $_3$ and Ca $^{2+}$

Recent structural insights have revealed PLC γ 1 in its autoinhibited state (18, 19), which is characterized by an inhibitory interface between the catalytic PLC core domains and the regulatory γ SA. To gain further structural insights, we have obtained a new structure of PLC γ 1, resolved to 2.0 Å, in its autoinhibited form and in the complex with IP $_3$ that has not been previously described for this PLC (Fig. 1A, fig. S1, and table S1). Our structure [Protein Data Bank (PDB) ID 7Z3J] reveals that the active site remains accessible to inositol phosphate, despite autoinhibition. The geometry of the active site is largely conserved compared to the structure of the related PLC δ 1—coordination of phosphate 1 of IP $_3$ involves H335, H380, and Ca $^{2+}$, the position 4 and 5 phosphates engage in electrostatic interactions, including interaction of the position 4 phosphate with K462 and R1010, and the 2-hydroxyl group is ligated to Ca $^{2+}$ (12). Despite the presence of excess IP $_3$ in the crystallization buffer, IP $_3$ binding to the nPH domain was not observed. This suggests that unlike PLC δ 1, the nPH of PLC γ 1 lacks a canonical PIP $_2$ binding site. Similarly, Ca $^{2+}$ binding to the C2 domain was not observed.

Although the overall fold is identical to the previously reported autoinhibited structure (PDB ID 6PBC), the PLC γ 1-IP $_3$ superimposes

with an overall root mean square deviation of 0.716 Å highlighting the dynamic nature of this multidomain enzyme, particularly for the γ SA. Furthermore, the new structure reveals detail for six newly resolved loops, resulting in the more complete structure (fig. S1). The two key regions of contact between the PLC core and the γ SA, which stabilize autoinhibition, are outlined in fig. S1B. First, there are hydrophobic, electrostatic, and hydrogen bonded contacts between the sPH and the TIM barrel, centered on the hydrophobic ridge near the entrance to the active site. A second interface is formed between the C2 and cSH $_2$ domains. M1166 and F1167, which form the hydrophobic tip of a loop on the C2 domain, bury into a hydrophobic pocket formed by F706, L746, and Y747 on the cSH $_2$ domain. There is additionally a weak interaction between the EF-hand and nSH $_2$ domains, stabilized by a single hydrogen bond between K175 and T576, which is positioned slightly differently from the previous structure (18).

Autoinhibition prevents liposome binding

To investigate how autoinhibitory interactions may affect recruitment of PLC γ 1 to membranes, we assessed the binding of either full-length PLC γ 1 (PLC γ^{FL}) or a core construct lacking the regulatory γ SA (Δ SA or PLC γ^{core}) to plasma membrane mimicking liposomes using a fluorescence resonance energy transfer (FRET)-based liposome binding assay. The PLC γ^{core} construct effectively bound to the liposomes under these conditions, but PLC γ^{FL} did not (Fig. 1B). To further investigate the binding of PLC γ^{FL} when autoinhibition is compromised by mutations, we used two variants (D1165H and S345F) previously characterized by an increase in basal PLC activity (36). In contrast to the wild-type (WT) PLC γ^{FL} , both variants bound to the liposomes, and the binding of D1165H variant was comparable to that of PLC γ^{core} (Fig. 1B). Consistent with recent models, these data suggest a mechanism where autoinhibition obstructs membrane binding by the PLC core and support the idea that the PLC γ^{core} construct interacts with membranes in a similar way as PLC γ^{FL} when fully activated (1, 18). These data are also consistent with observations that the PLC γ^{core} is both required and sufficient for maximal PLC activity (37–39). Consequently, the understanding of precise membrane interaction sites of the PLC γ^{core} , compared to autoinhibitory interfaces, could reveal key properties of an active PLC γ at the membrane and provide further insights into the mechanism of activation.

Characterizing the preferred membrane-bound orientation of the PLC γ 1 core

To characterize the membrane interaction of the PLC γ 1 core, high-throughput coarse-grained (CG) MD simulations were conducted (Fig. 2A). A model of the PLC γ 1 core domain was placed in a simulation box with a symmetric phosphoinositide-containing membrane model. The protein was placed above the membrane at a sufficient distance such that no forces from the membrane were experienced initially. Forty replicate simulations were generated with different initial velocities and run for 3 μ s, allowing convergence in simulation data (fig. S2). Stable membrane binding was observed in all but one replicate, at a center of mass z -axis separation of the protein and the bilayer of about 4 to 5 nm (fig. S3).

The orientation of the PLC γ 1 core throughout the simulation was quantified by measuring the angle (θ) between the z axis and a plane defined by the C α particles of residues 416, 1011, and 1194 (fig. S4). Before encountering the membrane, the PLC γ 1 core diffused freely in solution, suggesting that the initial geometry did not bias the subsequent membrane interaction (fig. S5). The selected backbone particles

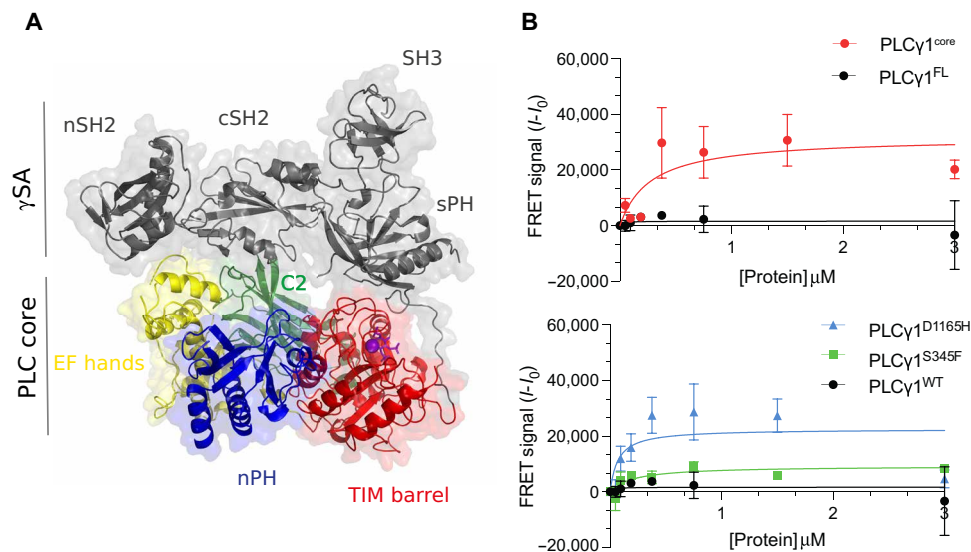


Fig. 1. Structure and liposome binding properties of PLC γ 1 variants. (A) The crystal structure of the IP₃/PLC γ 1 complex in an autoinhibited form (PDB ID: 7Z3J) with the domains of the PLC γ 1-specific array (γ SA) shown in gray and the domains in the PLC core colored individually (TIM barrel, red; nPH, blue; EF hands, yellow; C2, green); calcium ion and IP₃ in the active site are shown in purple. (B) Comparison of different variants of PLC γ 1 for interaction with liposomes. The full-length (FL) and PLC core (core) are shown in the top, and the FL variants with indicated mutations and the WT are shown in the bottom.

are in structured regions of the protein, and it is valid to assume minimal relative movement of these particles, due to the protein elastic restraint network used in the CG simulations. The plane was deliberately chosen to lie approximately parallel to the autoinhibitory interface observed in the PLC γ 1^{FL} structure. Therefore, if the proposed mechanism of autoinhibition by obstruction of the membrane-binding interface of the core domains is correct, then a preferred membrane-bound orientation with small value of θ would be expected. Analysis of θ and the protein-membrane z -distance over all simulation frames reveals that the PLC γ 1 core adopts a preferred membrane-bound orientation, with θ between 6° and 12° (Fig. 2B). Notably, this orientation positions the active site in productive contact with the membrane. Small populations of two alternative membrane-bound states were also observed. As these lowly populated alternative orientations position the active site away from the membrane, they are not likely to be physiologically relevant, although they may represent modes of interaction while PLC γ 1 is bound to receptor tyrosine kinases (RTKs) and in proximity to the membrane.

Examining how the density of different particle groups was distributed along the z axis of the system in the preferred orientation (Fig. 2C), we found that the side chains of residues F344, L384, and L1018 of the TIM barrel hydrophobic ridge insert into the membrane interior, with the density penetrating into the region of the phospholipid tails. Membrane insertion of this ridge near the entrance of the active site has been previously suggested for PLC δ 1, and the essential requirement for the PLC γ 1 F344 has been demonstrated by the loss of PLC activity in the F334A variant (12, 40, 41). However, interactions with lipids at the ridge have not been defined at the molecular level. Furthermore, our analysis revealed membrane insertion of M1166 and F1167, located at the hydrophobic tip of a loop on the C2 domain, which is a previously undescribed feature of the PLC γ 1 membrane interaction. Crucially, these two hydrophobic regions of the PLC γ core are involved in close contact with the γ SA in the full-length autoinhibited structure. Previous studies of PLC γ 1 disease-linked

mutations, affecting M1166 and F1167 residues, suggest their potential impact on both processes (18).

Overall, the preferred membrane-binding interface (Fig. 2D) aligns with the autoinhibitory interface and is characterized by membrane insertion of the TIM barrel hydrophobic ridge and C2 hydrophobic loop. The nPH, EF hands, and part of the TIM barrel skim the surface of the membrane, and the enzyme is positioned productively, due to contact of the active site and hydrophobic ridge with the membrane.

Identifying key sites for lipid interactions

Analysis of lipid contacts revealed hotspots for lipid interactions along the membrane-binding interface and an overall preference for interaction with phosphoinositides (fig. S6). In particular, we observed strong contacts with phosphoinositides on the nPH (β 1- β 2, β 3- β 4, and β 5- β 6 regions), EF hands (α 1 and the surrounding loops), and helices (α 5 and α 5') of the TIM barrel near the hydrophobic ridge (Fig. 3A). This result implies an unexpected mode of membrane interactions for the nPH and a role for the EF hands in membrane binding, not proposed before for PLC γ enzymes (18, 26). The structural basis for these phosphoinositide interaction hotspots are clusters of cationic lysine and arginine residues that point toward the membrane surface and interact with anionic lipid headgroups.

In addition to electrostatic interactions with anionic lipids, we observed hotspots for contact with cholesterol on the C2 hydrophobic loop and the TIM barrel hydrophobic ridge (Fig. 3B), which reflects the insertion of these regions into the membrane as described above. Other domains, such as nPH and EF hands, show considerably less interaction with cholesterol. On the basis of these results, we propose a model of PLC γ 1 core membrane binding, in which the C2 and TIM barrel domains undergo hydrophobic insertion into the membrane, while the nPH, EF hands, and a TIM barrel helix contribute to the membrane-bound state through electrostatic interactions with phosphoinositides and other anionic lipids at the membrane surface.

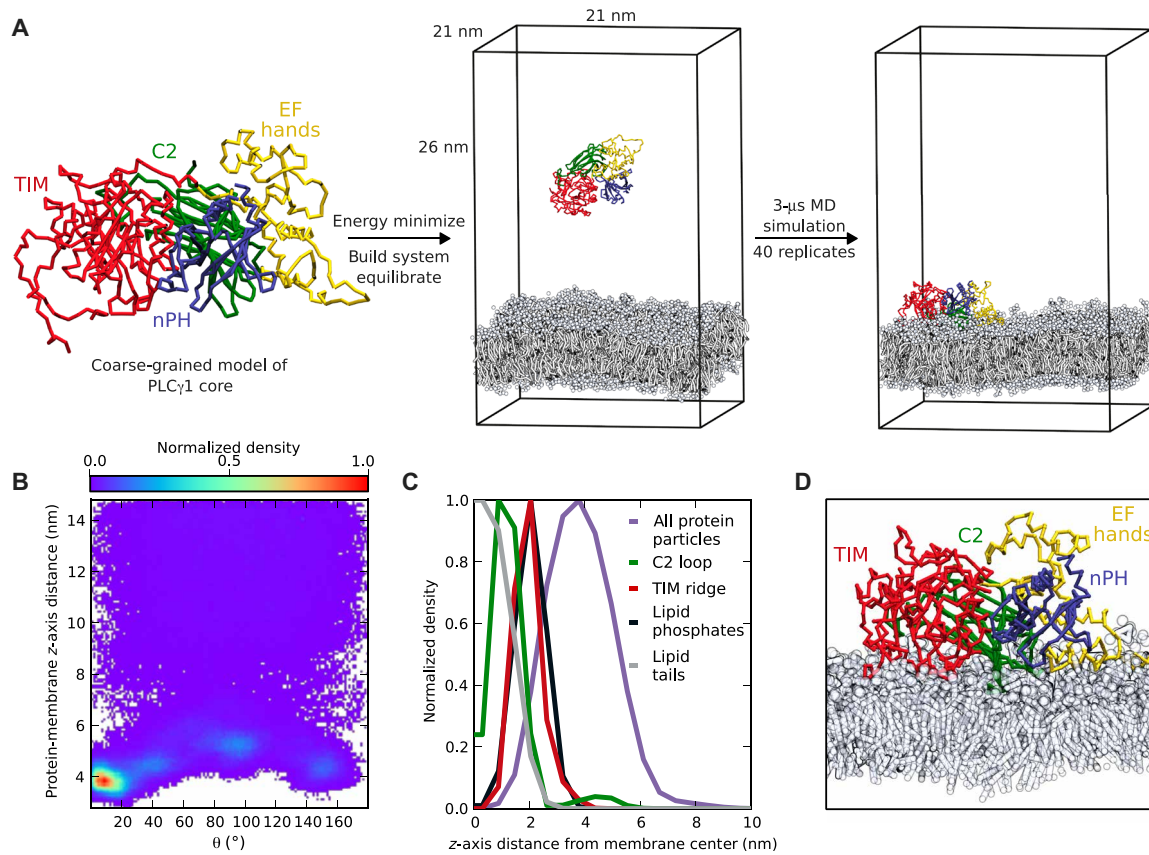


Fig. 2. Characterization of membrane interaction of the PLC γ 1 catalytic core using in silico techniques. (A) Schematic of the high-throughput CG MD simulation workflow used to study the membrane interactions of the PLC core. A CG model of PLC γ 1^{core} was placed in a simulation box with explicit solvent, ions, and a symmetric model lipid bilayer (containing POPE, POPC, POPS, PIP₂, PIP₃, and cholesterol) and equilibrated. Starting with the same initial geometry but differing initial velocities, 40 replicate MD simulations of 3- μ s duration were conducted using the Martini force field. Water molecules are omitted from the figure for clarity. (B) Two-dimensional histogram over all simulations, showing the density of states observed on a grid of protein-membrane distance and protein orientation (θ). (C) Distribution of protein groups along the z axis of the system in the preferred membrane-bound state. (D) Snapshot of the preferred membrane-bound state (at CG resolution), which positions the active site in contact with the membrane.

Basic residues in the nPH, EF-hand, and TIM barrel domains are crucial for the affinity and orientation of the PLC γ 1 core on the membrane

The clusters of basic residues that point toward the membrane surface, involved in electrostatic interactions, could be critical for the overall membrane binding. Therefore, we extended our analyses, including different experimental approaches, to investigate this new hypothesis. On the basis of contacts observed during simulations, we identified the most important residues for interaction with anionic lipids on the nPH (K41, K42, and R45), EF hands (R166, K175, R195, and R204), and TIM barrel (K990) domains. To test whether these residues are important for membrane binding and productive catalytic activity of PLC γ 1, we conducted further in vitro, in cell, and in silico studies using a panel of PLC γ 1 core constructs that contain lysine/arginine to alanine substitutions at the identified residues. An initial finding related to phosphoinositide/anionic lipid head-group affinity, based on Heparin Sepharose mobility, demonstrated decreasing affinity for negatively charged heparin with each additional mutation (fig. S7). We focused on three variants: (i) the core with the WT residues, designated as core WT; (ii) the core with the three substitutions in the nPH domain, designated as core P; and

(iii) the core with all eight substitutions, designated as core E. FRET liposome binding assays [performed with catalytically inactive versions (H335A)] demonstrated that the core WT construct has a preference for PIP₂-containing liposomes over liposomes containing anionic PS but not phosphoinositides (Fig. 4A). The core P mutant has reduced affinity for liposomes. This demonstrates the importance of the identified nPH residues (which lie outside the canonical PIP binding pocket for PH domains) for membrane affinity and phosphoinositide targeting. The core E variant displayed minimal binding to liposomes without PIP₂ and greatly reduced binding to PIP₂-containing liposomes compared to the core WT. The same variants of the PLC γ 1 core were also assessed for their PLC activity using different assay systems (Fig. 4, B to D, and fig. S8). When presented with liposome-bound substrate, the PLC activity was reduced by almost 50% in core P and by more than 90% for core E, relative to core WT (Fig. 4B and fig. S8A). In contrast, the activity toward soluble substrate was retained for both mutants (Fig. 4C and fig. S8B), indicating that the loss of activity is caused by reduction in membrane affinity and not loss of integrity of the active site. Furthermore, these findings are supported by reduction of activity of core P and core E observed in the cellular context (Fig. 4D and fig. S8C). These

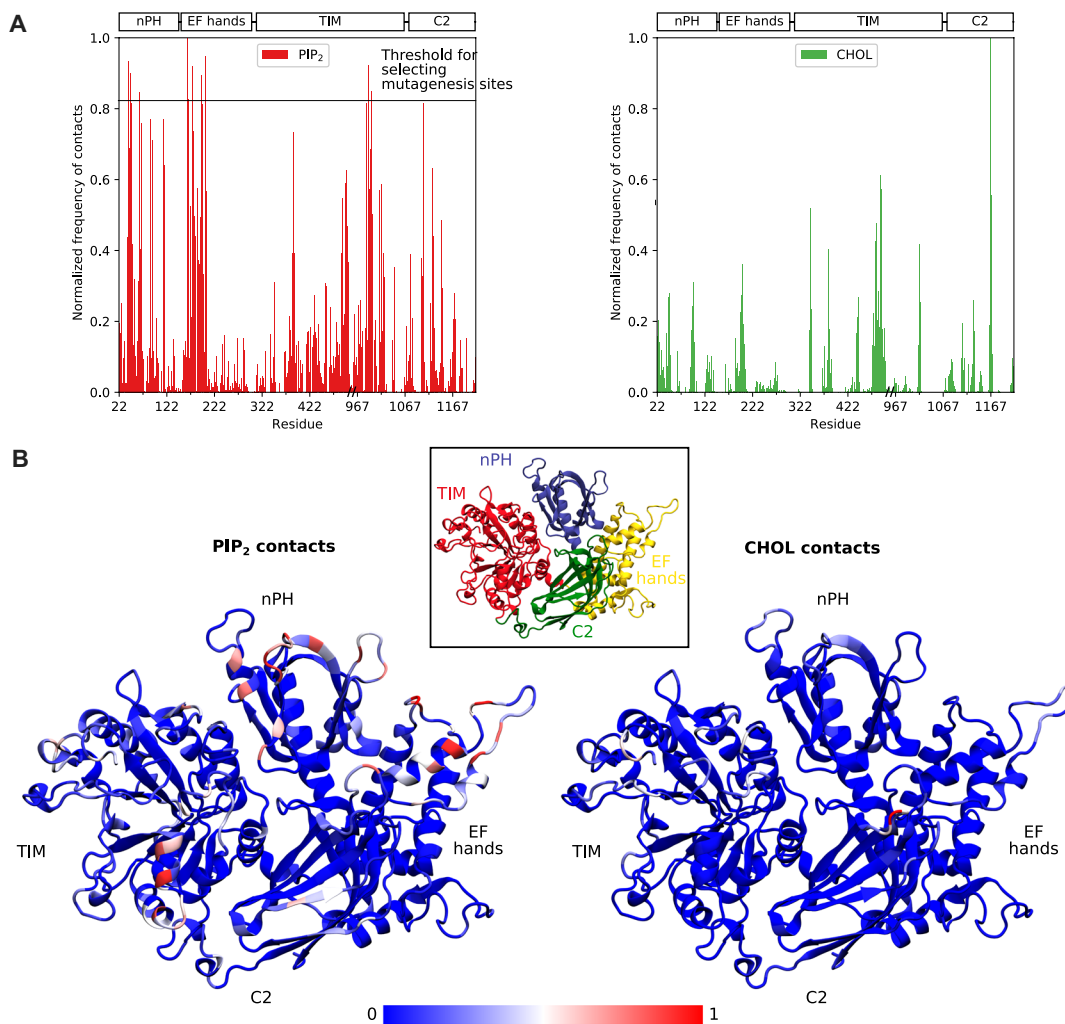


Fig. 3. Key sites for interaction with PIP₂ and cholesterol on PLC γ 1^{core}. (A) Normalized frequency of contacts with PIP₂ headgroups (red) or cholesterol (green). Contacts were tallied across all simulation frames of the final 1 μ s of simulation and normalized by dividing the total contacts at all residues by the total contacts for the residue with the most contacts. Residues with normalized PIP₂ headgroup contacts above 0.8 were considered to be the most important residues for electrostatic interaction with anionic lipids and selected for mutation in subsequent experiments. (B) Data in (A) mapped onto the PLC γ 1^{core} structure, where each residue is colored by its normalized frequency of contacts according to the blue-white-red scale shown. Inset: Structure of PLC γ 1^{core} colored by domain.

experimental data are consistent with further MD simulations of the mutants. Compared to core WT, simulations conducted using a core E model showed a depopulation of the preferred membrane-bound orientation (Fig. 4E) and a reduction in lipid contacts (Fig. 4F)—consequences of reduced membrane affinity and diminished ability to maintain a catalytically productive orientation without the crucial electrostatic interactions with anionic lipids.

An atomistic model of the PLC γ 1 core on the membrane

An atomistic model of the PLC γ 1 core on the membrane, with PIP₂ at the active site, was obtained by backmapping of the bound CG system to an all-atom representation for the CHARMM36 force field (fig. S9). The membrane-bound system was simulated for 1 μ s of atomistic simulation, during which time the PLC γ 1 remained bound to the membrane in the identified preferred orientation. From this simulation, we present the first atomistic model of the PLC core at the membrane surface, bound to its PIP₂ substrate (Fig. 5A). Examination

of the active site (Fig. 5B) revealed a solvent-accessible cavity that accommodates the PIP₂ headgroup, while the lipid acyl tails slot into a groove formed by the hydrophobic ridge. The hydrophobic ridge is inserted into the membrane and has additional interactions with cholesterol and the acyl tails of other phospholipid molecules. The dual nature of the active site—consisting of the solvent-accessible spout and hydrophobic ridge—allows accommodation of the amphiphilic lipid substrate and likely presents two separate exit pathways for the inositol phosphate (hydrophilic) and diacylglycerol (hydrophobic) reaction products, as has previously been suggested (12).

Details of interaction between the PIP₂ headgroup and the active site residues, shown in Fig. 5C and aligned in fig. S10A, are consistent with those seen for the IP₃ in the crystal structure (Fig. 5C, inset, and fig. S10A). The PIP₂ headgroup observed in the simulations, however, is not as deep in the active site as observed for IP₃ in the structure. To date, no structure of a PLC has been solved in complex with a complete lipid (only the inositol phosphate), and our model

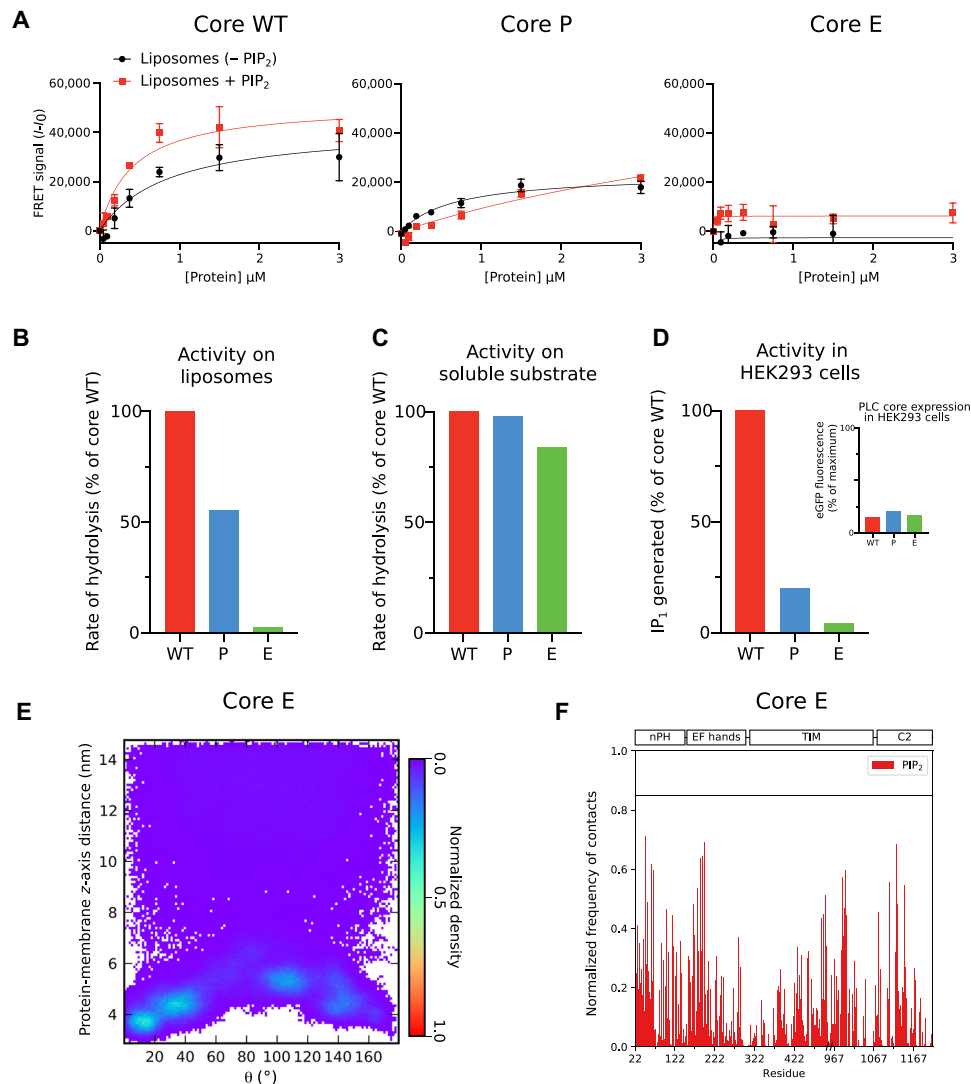


Fig. 4. The identified lipid interaction sites are critical for the membrane binding and the activity of PLC γ 1^{core} on membrane-bound substrate. (A) FRET intensity between PLC γ 1^{core} constructs and the fluorescent dansyl-phosphatidylserine (dPS) lipid probe embedded in PIP₂-containing liposomes (red traces) or liposomes lacking PIP₂ but which still contain anionic PS lipids (black traces). Data are shown for the PLC γ 1 core WT and variants with alanine substitutions of arginine/lysine residues in the nPH (core P) and combine eight substitutions for the entire core (core E). (B) Relative rate of hydrolysis of liposome-embedded phosphatidylinositol (PI) by the PLC γ 1^{core} constructs. The quantity of IP₁ produced was measured at multiple time points using HTRF with the addition of a labeled IP₁ probe and an anti-IP₁-labeled cryptate antibody. Initial hydrolysis rates calculated by linear regression and normalized to the core WT. (C) Relative rate of hydrolysis of soluble Aldol 518 myo-inositol-1-phosphate (Aldol) by the PLC γ 1^{core} constructs, monitored by measuring fluorescence of the reaction product. Equivalent enzyme concentrations that gave a linear activity were chosen, and the activity was presented as histograms for each variant normalized to the core WT. (D) Relative quantity of IP₁ generated in human embryonic kidney (HEK) 293 cells lysed 49 hours after transfection with enhanced green fluorescent protein (eGFP)-tagged PLC γ 1^{core} variants (core WT, core P, and core E). IP₁ produced was quantified using the HTRF assay previously described. Inset: Core variant expression levels presented as histograms showing the eGFP fluorescence normalized to the maximum eGFP expressed in a control well in the experiment. (E) Density of protein-membrane distance and orientation (θ) states observed in simulations of a PLC γ 1^{core} variant, core E. (F) Normalized frequency of contacts of core E with PIP₂ headgroups during simulation; the PIP₂ contacts are substantially reduced relative to core WT, as indicated by the original threshold line.

provides such a structure. It is possible that the interactions of the lipid tails with the hydrophobic ridge result in this small difference by preventing deeper penetration of the headgroup. On the other hand, our model of the active site geometry may not be fully optimized because of force field limitations and difficulty sampling such a large and computationally demanding simulation system. To overcome this limitation, further restrained MD simulations were conducted, with four distance restraints (see Materials and Methods) applied

between the PIP₂ headgroup and the protein based on the geometry of the inositol group observed in the structure. During the restrained simulations, the PIP₂ headgroup quickly moved deeper into the active site to match the geometry of inositol observed in the crystal structure (fig. S10B). The lipid acyl tails remained in contact with the hydrophobic ridge and did not perturb the ridge or the rest of the active site.

To obtain the atomistic model, it was important not to include the two linkers between the TIM barrel and the sPH domain

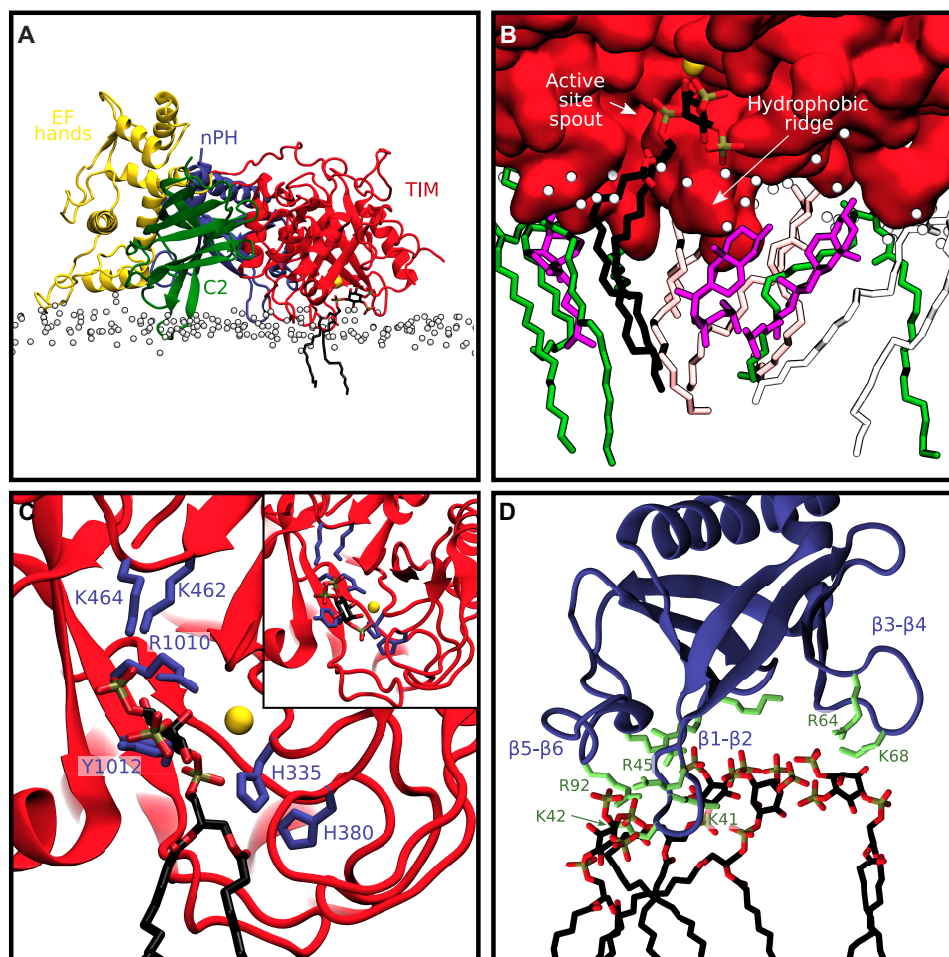


Fig. 5. A model of PLC γ 1^{core} at the membrane based on atomistic MD simulations. (A) Simulation snapshot of the PLC γ 1^{core} domains (nPH, blue; EF hands, yellow; TIM, red; C2, green) bound to the membrane with PIP₂ (stick representation) and Ca²⁺ (yellow sphere) at the active site. P1 lipid phosphate particles are shown as white spheres. (B) Overview of the active site (TIM barrel domain shown as red surface representation) with bound PIP₂. The hydrophobic ridge interacts with the tails of a number of additional lipid molecules (cholesterol, purple; POPE, green; POPC, salmon; POPS, white). (C) Zoom on the active site in the simulation snapshot, with notable residues (blue sticks) interacting with the PIP₂ headgroup. Inset shows the crystal structure of PLC γ 1 with IP₃ in the active site (see fig. S10A for detail). (D) View of the nPH domain interacting with multiple phosphoinositides at noncanonical sites during the simulation. Lysine and arginine residues are shown as green sticks.

(residues 471 to 488 and 934 to 947) during CG simulations, as we observed a tendency of these loops to move toward the active site and occlude entry of PIP₂ (fig. S9). To see whether the linker region prevents substrate access to the active site, the end frame of one of the simulations including the loops was selected (due to the presence of a PIP₂ molecule proximal to the active site in the preferred orientation), the linker loop residues were removed, and the CG simulation was extended for a further 1 μ s. During this simulation, PIP₂ entered and remained stably bound in the active site (fig. S9); this was used as the starting point for backmapping to the atomistic representation described above. The XY-linker loop of the PLC β family is known to inhibit substrate access to the active site in the inactive form of PLC β , and this may also be the case for the TIM barrel/sPH loops in the PLC γ family. This predicted occlusion occurs because of the specific loop positioning in the context of an autoinhibited enzyme, while the PLC γ ^{core} containing these loops retains high, constitutive PLC activity (38, 39). Alternatively, the observed active site occlusion could be an artifact of the CG simulation method, which has

limited accuracy in modeling conformational dynamics, and a tendency to overestimate protein-protein interactions (42).

In addition to insights into the TIM barrel active site binding to PIP₂, we have also obtained further detail for the C2 domain insertion, centered on M1166 and F1167. Structural and sequence alignment of the PLC γ 1 C2 domain and PLC δ 1 C2 domain (fig. S11A) suggests that the PLC γ 1 C2 domain may have lost Ca²⁺ binding functionality, and no Ca²⁺ binding was observed in the crystal structure, at this region, despite excess Ca²⁺. D653 in PLC δ 1 has previously shown to be essential for Ca²⁺-binding, yet in PLC γ 1, this position is replaced by a cysteine (fig. S11A) (43, 44). Furthermore, comparable residues to the membrane-inserting M1166 and F1167 of PLC γ 1 are not found in the PLC δ 1 loop regions. Together, these analyses suggest divergence in the mode of membrane interaction of the C2 domains in these two families. Further detail for the EF hands, highlighting interactions with anionic lipids, has also been obtained (fig. S11B). Involvement of the EF hands in membrane interactions, including binding to anionic lipids and PIP₂ mediated by arginine

and lysine residues, has been suggested for PLC δ 1 and PLC ζ 1; however, these protein/lipid interactions have not been precisely mapped (45, 46).

The nPH interacts with anionic lipids at multiple noncanonical sites

During simulations, we observed the nPH interacting with multiple anionic lipids at noncanonical sites (Fig. 5D). These interactions are facilitated by clusters of basic residues that point toward the membrane surface and engage in hydrogen bonding and electrostatic interactions with anionic lipid headgroups. K42, K45, and R92 comprise one binding site between the β 1- β 2 and β 5- β 6 loops. A second binding site is formed by R64 and K68, and a further region, which accommodates multiple lipid headgroups, is formed by K41, R88, R117, and K118 toward the back of the PH domain as shown in Fig. 5D. Two disease-linked mutations (E47K and R48W) in the nPH are outside these regions and have very little or no effect on the PLC γ 1 activity (18, 36, 47).

Structural alignment and comparison with previous simulations of the PLC δ 1 and ArhGAP9 PH domains (fig. S12) suggest that PLC γ 1 lacks the lysine and arginine residues present in the canonical pocket of PLC δ 1 PH and which appear to be necessary for strong and specific PIP₂ binding and in some other PH domains for the binding of PIP₃ (34). The PLC γ 1 nPH is more akin to the ArhGAP9 PH domain, which points clusters of basic residues outward toward the membrane, and has a noncanonical PIP binding pocket between the β 1- β 2 and β 5- β 6 loops (48). This analysis reconciles our findings that the nPH is critical for liposome binding and catalytic activity (Fig. 4, A to D) and yet has no IP₃ binding site detected in the crystal structure. Rather than specific strong binding to PIP₂, we propose that it contributes to membrane association through electrostatic interaction with multiple anionic lipids. In contrast to previous observations (26), a selective binding of PIP₃ to a canonical binding pocket is also unlikely.

Identifying possible interfaces of γ SA-membrane interaction

The positioning of the γ SA domains in the active form of PLC γ 1 is unknown, and it is possible that at least some of the γ SA could contribute toward membrane interaction. To identify the likely interfaces of such potential membrane interactions, further CG membrane-binding simulations were conducted for the structures of the sPH domain, tandem nSH2-cSH2, and the SH3 domain. We note that these simulations do not provide a measure of the strength of the membrane interaction but rather identify the most plausible mode of membrane interaction should it occur. For each structure, 20 replicate simulations of 1 μ s were conducted. As an indicator of the membrane-binding interface, we examined the normalized frequency of contacts with POPE headgroups for each structure (fig. S13). The sPH domain interacted with the membrane primarily through its C-terminal α -helix, which points a cluster of basic residues toward the membrane surface; PH domains typically interact at the opposite, open face of the β -barrel. This interaction is physiologically plausible as the sPH is likely to be positioned close to the membrane in the active form. For the cSH₂ domain, membrane interactions were localized around its phosphotyrosine binding site. In the active form, this region would be bound to the segment of cSH₂/SH₃ linker surrounding pY783; therefore, it is not likely to be a physiological site of membrane interaction (39, 49). In contrast with the PLC core, overall, the γ SA domains do not use the same interface for autoinhibition and membrane interaction.

DISCUSSION

Insights into the mechanisms by which PLC γ enzymes are activated and recruited to the plasma membrane are critical for understanding their roles in physiology and disease as well as for therapeutic intervention. By combining MD simulations with experimental approaches, we here elucidate key properties of membrane interactions by the PLC γ 1 catalytic core domains, resulting in productive substrate hydrolysis by an active enzyme. Our findings are summarized in the context of an overview for PLC γ activation (Fig. 6).

Among PLCs, PLC γ 1 and PLC γ 2 are uniquely characterized by a large regulatory array (γ SA) inserted between the X and Y boxes of the TIM barrel domain, and they are the only PLCs known to be activated via tyrosine phosphorylation (1). Furthermore, compared to other PLC families, the interactions between the regulatory domains and the PLC core are quite extensive resulting in strong autoinhibition. Although the PLC core is shared with other PLC families and has similar overall architecture, domains in the PLC core can have specific binding properties for various regulatory proteins or other ligands, distinct from those commonly recognized by these modular domains in other proteins. For example, in contrast to PIP₂ binding by the PLC δ 1 PH domain, the PH domain from PLC β 2 mediates binding of the small guanosine triphosphatase Rac (13). Similarly, Ca²⁺ binding by the EF hands has not been generally documented for PLC enzymes; instead, the EF hands in PLC β enzymes underpin the function that accelerates guanosine triphosphate hydrolysis by G α q, and in PLC δ 1 and PLC ζ 1, facilitate membrane interactions (45, 46, 50). Therefore, it is important to determine specific functional properties for the core domains in each PLC family. Overall, our data reveal such distinct functional properties of PLC γ 1 core domains with respect to membrane interactions. We show that multiple defined points of membrane interaction act in synergy, incorporating both hydrophobic and electrostatic components, and result in a productive orientation of the core on the membrane, with the PIP₂ substrate bound to the active site. (Figs. 3 to 5). Consistent with previous data for other PLC families (12), we found that the hydrophobic ridge of the TIM barrel inserts into the membrane and, in fact, forms a channel that accommodates the lipid tail (Fig. 5). Furthermore, we identified a previously unknown membrane-inserting loop on the C2 domain (Figs. 2C and 3 and fig. S11). With respect to interaction with inositol lipids and other anionic lipids, we show that the nPH helps to drive membrane association not via a canonical binding pocket for inositol lipids, as found for the PLC δ 1 PH domain, but through electrostatic interaction with multiple anionic lipid headgroups at noncanonical sites (Figs. 4 and 5 and fig. S12). Last, we found that the EF hands also drive membrane association through similar interactions with anionic lipids (Fig. 3 and fig. S11); no role of the EF hands in PLC γ has been previously identified. These membrane-targeting functions of the nPH and EF hands are crucial for the membrane binding and activity of PLC γ 1. The membrane interactions of the PLC core are summarized in Fig. 6 (inset).

Considering the unique autoinhibitory regions on the core of PLC γ 1, it is interesting that membrane-interacting surfaces, revealed in detail in this study, largely overlap with autoinhibitory interfaces (fig. S14). Key residues (K175, F344, L384, L1018, M1166, and F1167) clustered in areas involved in PLC core/ γ SA contacts in the autoinhibited structures were found to be important sites of membrane interactions also. Our data, therefore, strongly support a mechanism of PLC γ 1 autoinhibition via an extensive obstruction of the membrane-binding surfaces on the PLC core. A substantial change

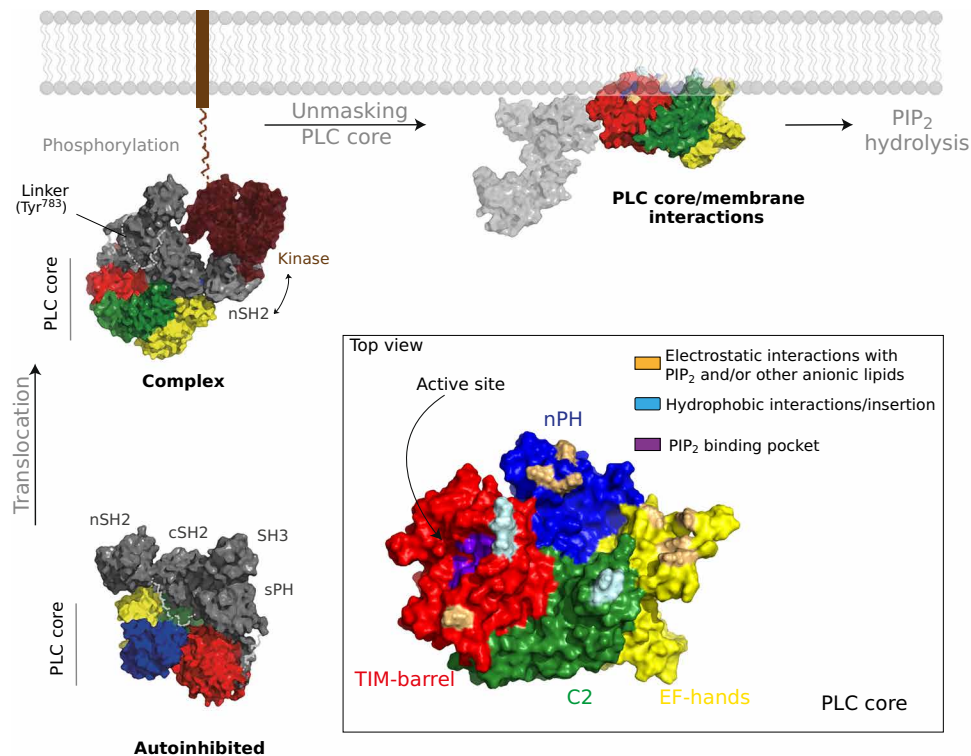


Fig. 6. Model for activation and membrane interactions of PLC γ 1. The depiction of the autoinhibited PLC γ 1 is based on crystal structures (PDB IDs: 6PBC and 7Z3J) (bottom left); it involves interactions between the regulatory region (γ SA) and the PLC core. In the best-defined activation route by RTKs (e.g., FGFR1), the translocation of PLC γ 1 to the membrane proximity is mediated by the recruitment to activated RTKs (e.g., FGFR1). The depiction of the PLC γ 1/FGFR1 complex is based on structural insights (EMD-10288 and PDB ID: 3GQI) (top left). The nSH2 domain in the γ SA binds to pTyr766 in the C-terminal tail of FGFR1. It is envisaged that subsequent destabilization of γ SA/PLC core interactions facilitates phosphorylation of Tyr⁷⁸³ in the cSH2/SH3 linker. Binding of pTyr⁷⁸³ to the cSH2 disrupts the cSH2/C2 autoinhibitory interface providing a key trigger for a large-scale rearrangement of the γ SA with respect to the PLC core. On the basis of our data, a complete “unmasking” of the PLC core surface is required for a productive orientation of the PLC core and the hydrolysis of membrane-resident PIP₂. In the depiction of PLC γ 1 at the membrane (top right), the γ SA position and shape are arbitrary (indicated by the light gray color). For the PLC core, the amino acid residues involved in interactions between the PLC core and the membrane, revealed here, are highlighted (inset).

upon activation must completely unmask the core surfaces, to produce a conformation that is competent for membrane binding. In addition to physiological activation, some of the strongly activating mutations could have a similar impact; we observed comparable liposome binding for PLC γ 1^{core} and PLC γ 1^{FL(D1165H)} variants (Fig. 1B), which supports the idea that activation exposes much of the inhibited core interface.

The overlap of the autoinhibitory and membrane-interacting interfaces in PLC γ extends the current framework for the mechanistic interpretation of the impact of various disease-linked mutations. For example, the activating S345F hotspot mutation in T cell lymphoma has been implicated in disruption of autoinhibitory sPH/TIM barrel interactions (18, 19). However, this mutation will also increase the hydrophobicity of the TIM barrel hydrophobic ridge and the loop regions that, based on our data (Fig. 5), interact with the acyl tails of PIP₂ bound at the active site. Similarly, considering this overlap, a rational design of potential inhibitors selective for PLC γ enzymes, by targeting unique features involved in membrane binding rather than the conserved active site, may result in disruption of the autoinhibitory regions and overall enzyme activation.

On the basis of the current evidence, the release of autoinhibitory interactions in PLC γ enzymes is mediated by protein-protein interactions and phosphorylation of the key tyrosine residue (Y783 in

PLC γ 1) (1). In the PLC β family, an additional role of the membrane interface in activation has been extensively studied (16, 21, 22, 51, 52). Specifically, a large cluster of acidic residues in the XY-linker occludes the active site and could be displaced in the proximity of the negatively charged membrane to enable access to PIP₂ substrate. The XY-linker from PLC β 2 can also inhibit the PLC γ ^{core} (38). Similar occlusion of the PLC γ 1 active site in the autoinhibited enzyme could involve the TIM barrel/sPH linkers (fig. S9); however, these linkers contain few negatively charged amino acid residues, and the repositioning of these linkers during activation is likely to be mechanistically different (38, 39). Although interfacial activation could play a role in regulation of PLC γ enzymes, this possibility and the precise mechanism remain unclear.

An overall activation mechanism for PLC γ enzymes presented in Fig. 6 mainly considers activation by RTKs and particularly the evidence obtained for the fibroblast growth factor receptor 1 (FGFR1)/PLC γ 1 interaction. Recently, studies of PLC γ activation in the context of signaling in immune cell types supported models with additional complexity related to different PLC γ conformations and interactions with adapter proteins, non-RTKs, and membrane mimetics (53–55). However, some of the common aspects of PLC γ membrane interactions remain unresolved. Notably, it is not clear whether the membrane-bound state, involving the PLC core/membrane

interactions, may be further stabilized by direct interactions of the γ SA domains with lipids (suggested by our simulations; fig. S13) or by indirect interactions with membrane-bound RTKs and adaptors. With respect to indirect interactions, our previous work has suggested that the active conformation of PLC γ 1 may be released from FGFR1 following phosphorylation and independently interact with the membrane (39). Nevertheless, the data obtained in this study reveal the contacts on the PLC core that are required for productive membrane orientation, regardless of other interactions by the entire PLC γ 1 protein. They also imply extensive rearrangements needed to unmask the PLC core surfaces that are involved in both complex autoinhibitory and membrane interactions. The insights gained here further support the capability of MD simulations to provide realistic and valuable insight into membrane biology (28, 56).

MATERIALS AND METHODS

Constructs, protein expression, and purification

Full-length human PLC γ 1 and its S345F and D1165H variants, cloned in the pTriEx4(Gateway) vector, have been described previously (19). Deletion variant lacking the γ SA regulatory region (amino acids 488 to 933), also referred to as PLC core, was generated using polymerase chain reaction as described previously (39). For constructs where PLC γ 1 was fused to enhanced green fluorescent protein (eGFP), an open reading frame (ORF) encoding eGFP was inserted N-terminally to the PLC γ 1 using ligation-independent cloning and verified by sequencing. All amino acid substitutions were generated using a site-directed mutagenesis kit (Agilent), and the ORFs of all clones were fully sequenced. The construct for protein crystallization of rat PLC γ 1 (98% amino acid identity with human PLC γ 1) included amino acids 21 to 765 and 791 to 1215, joined by a SGS linker, as originally described (18). The construct contains a TeV protease recognition sequence that after cleavage leaves two nonnative amino acid residues at the N terminus (serine and glutamine).

All PLC γ 1 proteins were expressed in *Escherichia coli* strain C41 (DE3). Cells were transformed, and colonies were grown up in 2xYT to an optical density at 600 nm of 0.5 at 37°C. Cultures were cooled for 2 hours at 15°C, and expression was induced by the addition of 100 mM isopropyl- β -D-thiogalactopyranoside and left overnight. Cells were harvested by centrifugation, and pellets were stored at -20°C until use.

Cell pellets from 1 liter of culture were lysed by the addition of 25 ml of lysis buffer [25 mM tris-Cl, 250 mM NaCl, 40 mM imidazole, 10 mM benzimidazole, 1 mM MgCl₂, and 100 ml of CaCl₂ (pH 8.0)] containing egg white lysozyme (0.25 mg/ml), with constant agitation at 4°C. After 30 min, 5 ml of 10% (v/v) Triton X-100 was added, and lysis was continued for another 30 min. Cell lysates were centrifuged for 1 hour at 20,000 rpm in a Beckman JA-25.50 rotor at 4°C.

Purification of crystallizable rat PLC γ 1

Clarified lysate was applied to a 5-ml HisTrap column on an Akta Purifier (Cytiva) system equilibrated in His buffer A [25 mM tris-Cl, 500 mM NaCl, 40 mM imidazole, and 1 mM TCEP (pH 8.0)] and washed for 20 column volumes in His buffer A to remove contaminants. Bound proteins were eluted with the addition of His buffer B [25 mM tris-Cl, 500 mM NaCl, 500 mM imidazole, and 1 mM TCEP (pH 8.0)]. The concentration of eluted protein was determined using Bradford reagent, and TeV protease was added giving a final ratio of TeV to protein of 1:50. The protein was dialyzed overnight at 4°C against 1 liter of dialysis buffer [25 mM tris-Cl, 20 mM NaCl, 10%

(v/v) glycerol, 1 mM TCEP, 1 mM EDTA, and 0.1 mM EGTA (pH 8.0)]. The following day, the protein was applied to a 5-ml HiTrap Heparin column (Cytiva) equilibrated in heparin buffer A [25 mM tris-Cl, 20 mM NaCl, and 1 mM TCEP (pH 8.0)] and washed with 4 column volumes of the same buffer. Proteins were eluted with a gradient over 20 column volumes with heparin buffer B [25 mM tris-Cl, 500 mM NaCl, and 1 mM TCEP (pH 8.0)]. Eluted PLC γ 1 was then injected onto a Superdex 200 preparative column (Cytiva) equilibrated in crystal gel filtration buffer [20 mM Hepes-NaOH, 150 mM NaCl, and 2 mM dithiothreitol (pH 7.5)], and 1 CV of an isocratic gradient resolved a peak of purified PLC γ 1. Proteins were concentrated to around 40 mg/ml using an Amicon Ultra-15 centrifugal filter unit (Merck) following the manufacturer's instructions, aliquoted, snap-frozen in liquid nitrogen, and stored at -80°C until use.

Purification of all other variants

Clarified lysate was applied to a 5-ml HisTrap column on an Akta Purifier (Cytiva) system equilibrated in His buffer A [25 mM tris-Cl, 500 mM NaCl, 40 mM imidazole, and 1 mM TCEP (pH 8.0)] and washed for 20 column volumes in His buffer A to remove contaminants. Bound proteins were eluted with the addition of His buffer B [25 mM tris-Cl, 500 mM NaCl, 500 mM imidazole, and 1 mM TCEP (pH 8.0)] and then diluted fourfold with dilution buffer [25 mM tris-Cl and 1 mM TCEP (pH 8.0)]. Diluted proteins were then applied to a 5-ml HiTrap Heparin column (Cytiva) equilibrated in heparin buffer A [25 mM tris-Cl, 20 mM NaCl, and 1 mM TCEP (pH 8.0)] and washed with 4 column volumes of the same buffer. Proteins were eluted with a gradient over 20 column volumes with heparin buffer B [25 mM tris-Cl, 500 mM NaCl, and 1 mM TCEP (pH 8.0)]. Eluted PLC γ 1 was then injected onto a Superdex 200 preparative column (Cytiva) equilibrated in gel filtration buffer [25 mM Hepes-NaOH, 150 mM NaCl, 5% (v/v) glycerol, and 2 mM TCEP (pH 7.5)], and 1 CV of an isocratic gradient resolved a peak of purified PLC γ 1. Proteins were generally concentrated to around 5 mg/ml using an Amicon Ultra-15 centrifugal filter unit (Merck) following the manufacturer's instructions, aliquoted, snap-frozen in liquid nitrogen, and stored at -80°C until use.

Protein crystallization

The protein for crystallization was prepared from a frozen stock (41 mg/ml). The protein was diluted to a final concentration of 7.0 mg/ml in the crystal construct gel filtration buffer, containing, in addition, 2 mM IP₃ and 2 mM CaCl₂. The crystallization experiment was set up immediately using a 24-well VDX crystallization plate (Hampton Research) and the hanging-drop vapor-diffusion technique. Equal volumes (1 μ l) of protein and reservoir solution were mixed against a 500- μ l reservoir solution at 20°C. A sparse matrix layout was designed for the crystallization trials by varying the concentrations of polyethylene glycol 3350 (PEG 3350) from 17 to 22% (w/v) and the pH of 0.1 M citric acid bis-tris propane (CBTP) buffer from 6.8 to 7.5. The best diffracting crystal for the complex was found in a condition containing 18.7% PEG 3350 and 0.1 M CBTP (pH 7.0). Before data collection, harvested crystals were immersed in a solution containing the precipitant mixture and 12% (v/v) 2-methyl-2,4-pentanediol and cryo-cooled in liquid nitrogen.

Crystallographic data collection and refinement

A crystal of the rPLC γ 1/IP₃ complex was measured at the ID23-1 beamline (ESRF, Grenoble, France) at 100 K and processed by the

XDS package (57). The crystal belonged to the $P 2_1 2_1 2_1$ space group with a solvent content of 52.9%, corresponding to one protein molecule in the asymmetric unit. The structure was determined by molecular replacement using MOLREP (58) using the previously determined structure of rPLC γ 1 with PDB ID 6PBC as a search model.

Initial rigid body refinement of the molecular replacement model using the phenix.refine program of the PHENIX suite (59) revealed extra density near the active site that was modeled as IP₃. Further iteration of TLS/maximum-likelihood refinement and manual model building and inspection using COOT (60), the model converged to a final $R_{\text{work}}/R_{\text{free}}$ of 0.2241/0.2551 at a maximum resolution of 2.00 Å. Data collection and refinement statistics are summarized in table S1.

Liposome preparation

Liposomes were prepared and stored at a final concentration of 2 mg/ml. The following lipid components in organic solvent were mixed in the following ratios for different liposomes:

- 1) Control FRET liposomes: 20% brain phosphatidylserine (PS), 40% brain phosphatidylethanolamine (PE), 15% brain phosphatidylcholine (PC), 10% cholesterol, 5% sphingomyelin, and 10% dansyl-phosphatidylserine (dPS) (w/v) (Avanti Polar Lipids).
- 2) PIP₂ FRET liposomes: 20% PS, 35% PE, 15% PC, 10% cholesterol, 5% sphingomyelin, 5% phosphatidylinositol (4,5) bisphosphate [PI(4,5)P₂], and 10% dPS.
- 3) PLC γ activity assay liposomes: 20% PS, 45% PE, 15% PC, 10% cholesterol, 5% sphingomyelin, and 5% phosphatidylinositol (PI).

The organic solvent was removed from the lipids in glass test tubes using a stream of nitrogen gas. The remaining solvent was removed by drying the lipids under vacuum for 2 hours at room temperature. Lipids were resuspended in liposome buffer [20 mM Hepes-KOH, 100 mM KCl, and 1 mM EGTA (pH 7.5)] by vortexing and bath sonication and then transferred to a microfuge tube. The liposomes were subjected to 11 freeze-thaw cycles between liquid nitrogen and a water bath at 42°C. Last, the liposomes were extruded through a 100-nm filter, and this process was repeated 10 more times. Liposomes were snap-frozen in liquid nitrogen and stored at -80°C.

Protein-liposome FRET assay

Liposome binding was monitored by observing the FRET interaction between an 18:1

dPS fluorescent lipid probe and intrinsic tryptophan fluorescence of the PLC γ 1 variants. Liposomes were defrosted and kept at room temperature until use. Assay components were diluted in FRET buffer [30 mM Hepes-NaOH and 50 mM NaCl (pH 7.5)]. Liposomes were diluted to 100 mg/ml. Proteins were diluted to a maximum concentration of 6 mM, and then a further sixfold dilution series was prepared. In a black, low binding 384-well plate (Greiner Bio-One), 5 ml of protein (or buffer only for I_0 measurements) and 5 ml of liposomes were mixed in triplicate. Plates were sealed and then incubated for 1 hour at room temperature. FRET was measured on a PHERAstar plate reader (BMG Labtech) using a 280-nm excitation filter and 350/520-nm emission filters to measure Trp and dPS emissions, respectively. The FRET signal shown in figures is $(I - I_0)$, where I is the intensity at 520 nm, and where I_0 is the intensity for a solution with lipid only (without protein). Binding curves were fit with a one site-specific binding curve using GraphPad Prism (Prism v9.3.0 for Mac). Association constants (K_d) have not been reported since PLC $\gamma^{\text{FL-WT}}$ did not display any measurable binding. Each analysis

was repeated twice (biological replicates) with three replicates in each experiment (technical replicates).

Measurement of PLC activity in vitro

Determination of PLC activity in vitro was performed by two methods. First, the PLC-driven hydrolysis of PI incorporated in liposomes was monitored by quantifying the production of inositol phosphate (IP₁) using the IPone kit (CisBio) in an end point assay format. Second, the real-time hydrolysis of the synthetic substrate Aldol 518 myo-inositol-1-phosphate (abbreviated to Aldol) (Biosynth) was monitored in a continuous assay format. Essentially, both methods used the following assay buffer [20 mM Hepes-KOH, 70 mM KCl, 3 mM EGTA, 2.97 mM CaCl₂, 2 mM TCEP, and fatty acid-free bovine serum albumin (BSA; 50 µg/ml) (pH 7.0)].

For the measurement of IP₁ production, liposomes containing PI as outlined above were thawed, diluted to lipid (0.2 mg/ml) in assay buffer, and stored at room temperature. The PLC proteins were assayed at a final concentration of 50 nM in a total assay volume of 150 µl. Samples of 15 µl were removed at various time intervals, and the reaction was stopped by the addition of 20 µl of stop buffer [50 mM EGTA and 0.6% (w/v) sodium cholate (pH 8.0)] and heat denaturation at 80°C for 2 min. The amount of IP₁ was quantified through the addition of a labeled IP₁ probe and an anti-IP₁-labeled cryptate antibody and monitored by Homogeneous Time Resolved Fluorescence (HTRF) as outlined in the manufacturer's instructions. The amount of IP₁ produced was calculated by interpolation from a standard curve. The initial rate of hydrolysis was calculated using linear regression and plotted as histograms for each variant normalized to the core^{WT} variant activity. Each analysis was repeated twice (biological replicates) with three replicates in each experiment (technical replicates).

In the continuous assay format, the enzymatic activity of core variants was quantified using the soluble Aldol substrate. Activity was measured in low-volume black 384-well plates (Greiner Bio-One). A final assay volume of 20 µl contained 25 µM Aldol substrate in assay buffer, 125 µM Aldol 355 fluorescence enhancer (Biosynth), and a serial dilution of PLC core variants. All were performed in triplicate. Production of fluorescent product was monitored in a CLARIOstar multimode plate reader (BMG Labtech) with an excitation filter of 510 nm and an emission filter of 618 nm. Equivalent enzyme concentrations that gave a linear activity were chosen, and the activity was presented as histograms for each variant normalized to the core^{WT} variant activity. Each analysis was repeated twice (biological replicates) with three replicates in each experiment (technical replicates).

Measurement of PLC activity in cells

For the measurements of PLC activity, human embryonic kidney (HEK) 293 cells were cultured in Dulbecco's modified Eagle's medium (Sigma-Aldrich) containing 10% (v/v) fetal bovine serum (FBS) and 2.5 mM glutamine (growth media). Cells were grown as a monolayer at 37°C in 5% CO₂. HEK293 cells were seeded into 96-well plates at a density of 7500 cells per well in 0.1 ml of growth media and incubated overnight. Fresh medium was applied, and the cells were transfected with plasmid DNA at 50 ng per well, which had been diluted in 5 µl of jetPRIME buffer and 0.2 µl of jetPRIME (Polyplus) that were prepared as instructed by the manufacturer. The DNA concentration was kept constant by adding empty plasmid. Each PLC γ 1^{core} construct was transfected at several concentrations in triplicate. Twenty-four hours after transfection, the media was removed and replaced with growth media without FBS but containing 0.25% (w/v)

fatty acid-free BSA. The HEK293 cells were then incubated for a further 24 hours. Subsequently, the media was replaced with growth media without FBS but containing 50 mM LiCl and incubated for a further 1 hour. The media was aspirated and replaced by 25 μ l of 2 \times stimulation buffer (CisBio) followed by 25 μ l of lysis buffer (CisBio). The cells were lysed for 10 min at room temperature on an orbital shaker. Fourteen microliters of the cell lysate was pipetted into white 384-well plates (Greiner Bio-One) followed by 3 μ l of IP1-d2 and 3 μ l of anti-IP1-cryptate (Cisbio). The plate was sealed and incubated at room temperature for 1 hour. The plate was read on a PHERAstar (BMG Labtech) plate reader in HTRF mode using a 337-nm excitation filter and 620/665-nm emission filters. The data were converted to IP1 concentration using a standard curve generated following the manufacturer's instructions.

Expressed PLC γ 1^{core} constructs were eGFP tagged. Therefore, the same plate analyzed for IP1 concentration was reread for recombinant protein expression using a CLARIOstar plate reader (BMG Labtech) with 470-nm excitation and 515-nm emission. PLC activity data are presented as histograms showing the IP1 generated normalized to the value for the core WT variant. Core variant expression levels are also presented as histograms showing the eGFP fluorescence normalized to the maximum eGFP expressed in a well in that experiment. Each analysis was repeated twice (biological replicates) with three replicates in each experiment (technical replicates).

CG MD simulations

CG MD simulations were conducted using the Martini v2.1 force field and GROMACS v5.0.7 (61, 62). A structural model of the core domains of PLC γ 1 (nPH, EF hands, TIM, and C2) was obtained from the autoinhibited structure by removing the coordinates for the sPH, nSH2, cSH3, and SH3 domains and remodeling missing atoms in loop regions using the program PRIME in the Schrodinger suite. The model used for CG simulations comprises residues 22 to 488 and 934 to 1215. A model of clone E was obtained by mutating residue 41, 42, 45, 166, 175, 195, 204, and 990 to alanine using MODELLER (63).

The WT core and the core^E (incorporating eight amino acid substitutions to alanine) models were converted to CG representations for the martini v2.1 force field using the martinize tool provided by the martini developers (64). Each CG protein was placed in a cubic periodic box of dimensions 21 nm by 21 nm by 26 nm, and energy minimized using the steepest descent method. The insane tool for computational lipidomics was used to construct a symmetric model membrane (composition: 40% POPE, 25% CHOL, 15% POPS, 10% POPC, 7% POP2, and 3% POP3), solubilize, and neutralize the system with Martini waters, sodium, and chloride ions (65). The system was energy-minimized using the steepest descent method and subjected to three rounds of equilibration in the NPT ensemble: for 20 ns with 5-fs time step, 1.5 ns with 7.5-fs time step, and then 2 ns with 10-fs time step. For all equilibrations, we used the velocity-rescaling thermostat at 323 K and the semi-isotropic Parrinello-Rahman barostat at 1 bar, and the protein backbone particles were restrained (66, 67). Production simulations were run for 3 μ s with 20-fs time step, using the velocity-rescaling thermostat (323 K) and semi-isotropic Parrinello-Rahman barostat (1 bar). Forty replicate production simulations for each protein were initialized from the equilibrated system, with velocities sampled from a Boltzmann distribution.

For simulations without the TIM barrel/sPH loops, WT core simulation replicate 39 was selected for extended simulation. The loop

residues (471 to 488 and 934 to 947; sequence AYEEVPTSVMYSENDISN and DARLTEGKMMERRK) and two sodium ions (to balance charge) were removed from the system, and an additional 1 μ s of simulation was conducted.

Simulations of the sPH, nSH2-cSH2, and SH3 domain structures were conducted and analyzed using the same methods as for the PLC γ 1 core, with adjustments due to the smaller protein sizes (simulation time: 1 μ s; number of replicates: 20; box dimensions: 16.5 nm by 16.5 nm by 20.5 nm).

Atomistic MD simulations

Conversion to an atomistic representation for the CHARMM36 force field was achieved using the backward method (68, 69). H335 and H380 were protonated, and a calcium ion was placed in the active site at the position observed in the crystal structure. The latest CHARMM36 lipid parameters were obtained from CHARMMGUI, with the Martini to CHARMM36 lipid type mappings described in table S2 (70). POPI25 was chosen as a model for PI(4,5)P₂ on the basis of ab initio studies, indicating that this is the preferred protonation state (71). The backmapped protein coordinates were replaced with those from the original atomistic PDB after superimposition upon the backmapped structure, to correct any structural changes occurring during CG simulation and backmapping. To ensure the correct headgroup stereochemistry of the active site PIP₂ after backmapping, the headgroup coordinates of this POPI25 were replaced by superimposition with those of a reference POPI25 obtained from a pure POPI35 membrane constructed using the CHARMM-GUI membrane builder (70). The backmapped protein and lipids were placed in a 19.6 nm by 19.6 nm by 16.5 nm cubic periodic box, energy-minimized (steepest descent), and subjected to 1 ns of equilibration with a 1-fs time step in the NPT ensemble, as described for the CG equilibrations. An unrestrained production simulation was run for 1 μ s, with a 2-fs time step, a temperature of 323 K, and a semi-isotropic Parrinello-Rahman pressure coupling at 1 bar (66, 67).

For restrained MD simulations to further investigate the geometry of PI(4,5)P₂ in the active site, harmonic distance restraints were applied between the following atoms of the bound PIP₂ and the protein: PIP₂:P1-HIS380:NE2; PIP₂:P1-HIS335:NE2; PIP₂:P4-LYS462:NZ; and PIP₂:O3-ARG988:CZ. Restraints were based on the distances observed in the IP3-bound crystal structure and are detailed in Supplementary Text. The restrained simulation was initiated from the end point of the 1- μ s unrestrained atomistic simulation and simulated for 10 ns, keeping all other settings the same.

Simulation analysis

For analysis, the protein was centered in the simulation box throughout the trajectories to prevent artifacts arising due to periodic boundary conditions (PBC). Root mean square deviation and root mean square fluctuation of protein backbone particles were calculated for each trajectory relative to its first frame. The GROMACS dist module was used to calculate the *z*-axis distance between the protein and membrane centers of mass. The protein orientation was determined by using the GROMACS gangle module to measure the angle (θ) between the plane defined by the backbone particles of residues 416, 1011, and 1194 and the *z* axis of the simulation box. The purpose of distance and orientation analysis was to understand the geometry of the protein relative to membrane, and hence, the measurements were corrected to account for PBC, which allowed the protein to bind to either leaflet of the membrane by traveling

through the periodic boundary on the z axis. PBC corrections were applied using the following equations for all simulation frames where $z\text{-dist}_{\text{uncorrected}} < 0$ (i.e., when the protein was below the membrane center of mass): $\theta = 180^\circ - \theta_{\text{uncorrected}}$ and $z\text{-dist} = -1 * z\text{-dist}_{\text{uncorrected}}$. Corrections were performed using Python before further analysis and visualization.

The distance-orientation density plot was generated as a two-dimensional histogram of z -distance and θ over all simulation frames. Particle z -axis density plots were constructed using `gmx density`, taking the symmetrized density along the z axis relative to the membrane center of mass for the following particle groups: phospholipid tails, phospholipid headgroups, C2 hydrophobic loop, TIM hydrophobic ridge, and protein. To ensure that this z -axis density analysis characterized only the identified preferred orientation of the core, it was conducted only for simulations that ended with a θ between 6° and 12° and protein-membrane z -axis distance < 4.5 nm and only for the final 500 ns of these simulations.

Contacts between all residues and all lipid particles were calculated using the following groupings for lipids: POPC headgroup, POPE headgroup, POPS headgroup, POP2 headgroup, POP3 headgroup, and CHOL. Using the GROMACS `mindist` module, we determined whether a molecule had particles belonging to the given lipid group and that were within a 5.5 \AA cutoff distance of any particles belonging to each protein residue. For each lipid molecule satisfying this criterion during a simulation frame, one contact was counted. Contacts were totalled over all frames during the final 1000 ns of each simulation, for each residue and lipid group. Normalized frequency of contacts was obtained by dividing the total contacts at each residue by the total contacts made by the residue with the highest number of contacts within that lipid group. Thus, the residue with the highest number of contacts has the normalized value 1, and the contacts for all other residues are normalized relative to this residue. Convergence analysis was carried out as above, using differently sized samples of simulation replicates.

Bioinformatic analysis

Structural alignments were conducted in VMD, using the STAMP method (72, 73). Sequence alignments were conducted in JalView, using the ClustalW method and canonical human PLC sequences obtained from UniProt (PLC γ 1: P19174; PLC δ 1: P51178; PLC ζ 1: Q86YW0) (74).

SUPPLEMENTARY MATERIALS

Supplementary material for this article is available at <https://science.org/doi/10.1126/sciadv.abp9688>

[View/request a protocol for this paper from Bio-protocol.](#)

REFERENCES AND NOTES

- M. Katan, S. Cockcroft, Phospholipase C families: Common themes and versatility in physiology and pathology. *Prog. Lipid Res.* **80**, 101065 (2020).
- M. Katan, S. Cockcroft, Phosphatidylinositol(4,5)bisphosphate: Diverse functions at the plasma membrane. *Essays Biochem.* **64**, 513–531 (2020).
- H. Koss, T. D. Bunney, S. Behjati, M. Katan, Dysfunction of phospholipase $C\gamma$ in immune disorders and cancer. *Trends Biochem. Sci.* **39**, 603–611 (2014).
- M. J. Ombrello, E. F. Remmers, G. Sun, A. F. Freeman, S. Datta, P. Torabi-Parizi, N. Subramanian, T. D. Bunney, R. W. Baxendale, M. S. Martins, N. Romberg, H. Komarow, I. Aksentijevich, H. S. Kim, J. Ho, G. Cruse, M. Y. Jung, A. M. Gilfillan, D. D. Metcalfe, C. Nelson, M. O'Brien, L. Wisch, K. Stone, D. C. Douek, C. Gandhi, A. A. Wanderer, H. Lee, S. F. Nelson, K. V. Shianna, E. T. Cirulli, D. B. Goldstein, E. O. Long, S. Moir, E. Meffre, S. M. Holland, D. L. Kastner, M. Katan, H. M. Hoffman, J. D. Milner, Cold urticaria, immunodeficiency, and autoimmunity related to PLCG2 deletions. *N. Engl. J. Med.* **366**, 330–338 (2012).
- S. Behjati, P. S. Tarpey, H. Sheldon, I. Martincorena, P. van Loo, G. Gundem, D. C. Wedge, M. Ramakrishna, S. L. Cooke, N. Pillay, H. K. M. Volland, E. Papaemmanuil, H. Koss, T. D. Bunney, C. Hardy, O. R. Joseph, S. Martin, L. Mudie, A. Butler, J. W. Teague, M. Patil, G. Steers, Y. Cao, C. Gumbs, D. Ingram, A. J. Lazar, L. Little, H. Mahadeshwar, A. Protopopov, G. A. al Sanna, S. Seth, X. Song, J. Tang, J. Zhang, V. Ravi, K. E. Torres, B. Khatri, D. Halai, I. Roxanis, D. Baumhoer, R. Tirabosco, M. F. Armary, C. Boshoff, U. McDermott, M. Katan, M. R. Stratton, P. A. Futreal, A. M. Flanagan, A. Harris, P. J. Campbell, Recurrent PTPRB and PLCG1 mutations in angiosarcoma. *Nat. Genet.* **46**, 376–379 (2014).
- Q. Zhou, G. S. Lee, J. Brady, S. Datta, M. Katan, A. Sheikh, M. S. Martins, T. D. Bunney, B. H. Santich, S. Moir, D. B. Kuhns, D. A. L. Priel, A. Ombrello, D. Stone, M. J. Ombrello, J. Khan, J. D. Milner, D. L. Kastner, I. Aksentijevich, A hypermorphic missense mutation in PLCG2, encoding phospholipase $C\gamma$ 2, causes a dominantly inherited autoinflammatory disease with immunodeficiency. *Am. J. Hum. Genet.* **91**, 713–720 (2012).
- J. A. Woyach, R. R. Furman, T. M. Liu, H. G. Ozer, M. Zapatka, A. S. Ruppert, L. Xue, D. H. H. Li, S. M. Steggerda, M. Versele, S. S. Dave, J. Zhang, A. S. Yilmaz, S. M. Jaglowski, K. A. Blum, A. Lozanski, G. Lozanski, D. F. James, J. C. Barrientos, P. Lichter, S. Stiglbauer, J. J. Buggy, B. Y. Chang, A. J. Johnson, J. C. Byrd, Resistance mechanisms for the Bruton's tyrosine kinase inhibitor ibrutinib. *N. Engl. J. Med.* **370**, 2286–2294 (2014).
- K. M. de Lange, L. Moutsianas, J. C. Lee, C. A. Lamb, Y. Luo, N. A. Kennedy, L. Jostins, D. L. Rice, J. Gutierrez-Achury, S. G. Ji, G. Heap, E. R. Nimmo, C. Edwards, P. Henderson, C. Mowat, J. Sanderson, J. Satsangi, A. Simmonds, D. C. Wilson, M. Tremelling, A. Hart, C. G. Mathew, W. G. Newman, M. Parkes, C. W. Lees, H. Uhlig, C. Hawkey, N. J. Prescott, T. Ahmad, J. C. Mansfield, C. A. Anderson, J. C. Barrett, Genome-wide association study implicates immune activation of multiple integrin genes in inflammatory bowel disease. *Nat. Genet.* **49**, 256–261 (2017).
- K. Kataoka, Y. Nagata, A. Kitanaka, Y. Shiraiishi, T. Shimamura, J. I. Yasunaga, Y. Totoki, K. Chiba, A. Sato-Otsubo, G. Nagae, R. Ishii, S. Muto, S. Kotani, Y. Watatani, J. Takeda, M. Sanada, H. Tanaka, H. Suzuki, Y. Sato, Y. Shiozawa, T. Yoshizato, K. Yoshida, H. Makishima, M. Iwanaga, G. Ma, K. Nosaka, M. Hishizawa, H. Itonaga, Y. Imaizumi, W. Munakata, H. Ogasawara, T. Sato, K. Sasai, K. Muramoto, M. Penova, T. Kawaguchi, H. Nakamura, N. Hama, K. Shide, Y. Kubuki, T. Hidaka, T. Kameda, T. Nakami, K. Ishiyama, S. Miyawaki, S. S. Yoon, K. Tobinai, Y. Miyazaki, A. Takaori-Kondo, F. Matsuda, K. Takeuchi, O. Nureki, H. Aburatani, T. Watanabe, T. Shibata, M. Matsuoka, S. Miyano, K. Shimoda, S. Ogawa, Integrated molecular analysis of adult T cell leukemia/lymphoma. *Nat. Genet.* **47**, 1304–1315 (2015).
- R. Sims, S. J. van der Lee, A. C. Naj, C. Bellenguez, N. Badarinarayan, J. Jakobsdottir, B. W. Kunkle, A. Boland, R. Raybould, J. C. Bis, E. R. Martin, B. Grenier-Boley, S. Heilmann-Heimbach, V. Chouraki, A. B. Kuzma, K. Sleegers, M. Vronskaya, A. Ruiz, R. R. Graham, R. Oloaso, P. Hoffmann, M. L. Grove, B. N. Vardarajan, M. Hiltunen, M. M. Nöthen, C. C. White, K. L. Hamilton-Nelson, J. Epelbaum, W. Maier, S.-H. Choi, G. W. Beecham, C. Dulary, S. Herms, A. V. Smith, C. C. Funk, C. Derbois, A. J. Forstner, S. Ahmad, H. Li, D. Bacq, D. Harold, C. L. Satizabal, O. Valladares, A. Squassina, R. Thomas, J. A. Brody, L. Qu, P. Sánchez-Juan, T. Morgan, F. J. Wolters, Y. Zhao, F. S. Garcia, N. Denning, M. Fornage, J. Malamon, M. C. D. Naranjo, E. Majounie, T. H. Mosley, B. Dombroski, D. Wallon, M. K. Lupton, J. Dupuis, P. Whitehead, L. Fratiglioni, C. Medway, X. Jian, S. Mukherjee, L. Keller, K. Brown, H. Lin, L. B. Cantwell, F. Panza, B. M. Guinness, S. Moreno-Grau, J. D. Burgess, V. Solfrizzi, P. Proitsi, H. H. Adams, M. Allen, D. Seripa, P. Pastor, L. A. Cupples, N. D. Price, D. Hannequin, A. Frank-García, D. Levy, P. Chakrabarty, P. Caffarra, I. Giegling, A. S. Beiser, V. Giedraitis, H. Hampel, M. E. Garcia, X. Wang, L. Lannfelt, P. Mecocci, G. Eiriksdottir, P. K. Crane, F. Pasquier, V. Boccardi, I. Hernández, R. C. Barber, M. Scherer, L. Tarraga, P. M. Adams, M. Leber, Y. Chen, M. S. Albert, S. Riedel-Heller, V. Emilsson, D. Beekly, A. Braae, R. Schmidt, D. Blacker, C. Masullo, H. Schmidt, R. S. Doody, G. Spalletta, W. T. Longstreth Jr., T. J. Fairchild, P. Bossù, O. L. Lopez, M. P. Frosch, E. Sacchinelli, B. Ghetti, Q. Yang, R. M. Huebinger, F. Jessen, S. Li, M. I. Kamboh, J. Morris, O. Sotolongo-Grau, M. J. Katz, C. Corcoran, M. Dunstan, A. Braddel, C. Thomas, A. Meggy, R. Marshall, A. Gerrish, J. Chapman, M. Aguilar, S. Taylor, M. Hill, M. D. Fairén, A. Hodges, B. Vellas, H. Soininen, I. Kloszewska, M. Daniilidou, J. Uphill, Y. Patel, J. T. Hughes, J. Lord, J. Turton, A. M. Hartmann, R. Cecchetti, C. Fenoglio, M. Serpente, M. Arcaro, C. Caltagirone, M. D. Orfei, A. Ciarabella, S. Pichler, M. Mayhaus, W. Gu, A. Lleó, J. Fortea, R. Blesa, I. S. Barber, K. Brookes, C. Cupidi, R. G. Maletta, D. Carrell, S. Sorbi, S. Moebus, M. Urbano, A. Pilotto, J. Kornhuber, P. Bosco, S. Todd, D. Craig, J. Johnston, M. Gill, B. Lawlor, A. Lynch, N. C. Fox, J. Hardy, ARUK Consortium, R. L. Albin, L. G. Apostolova, S. E. Arnold, S. Asthana, C. S. Atwood, C. T. Baldwin, L. L. Barnes, S. Barral, T. G. Beach, J. T. Becker, E. H. Bigio, T. D. Bird, B. F. Boeve, J. D. Bowen, A. Boxer, J. R. Burke, J. M. Burns, J. D. Buxbaum, N. J. Cairns, C. Cao, C. S. Carlson, C. M. Carlsson, R. M. Carney, M. M. Carrasquillo, S. L. Carroll, C. C. Diaz, H. C. Chui, D. G. Clark, D. H. Cribbs, E. A. Crocco, C. DeCarli, M. Dick, R. Duara, D. A. Evans, K. M. Faber, K. B. Fallon, D. W. Fardo, M. J. R. Farlow, S. Ferris, T. M. Foroud, D. R. Galasko, M. Gearing, D. H. Geschwind, J. R. Gilbert, N. R. Graff-Radford, R. C. Green, J. H. Growdon, R. L. Hamilton, L. E. Harrell, L. S. Honig, M. J. Huentelman, C. M. Hulette, B. T. Hyman, G. P. Jarvik, E. Abner, L.-W. Jin, G. Jun, A. Karydas, J. A. Kaye,

- R. Kim, N. W. Kowall, J. H. Kramer, F. M. LaFerla, J. J. Lah, J. B. Leverenz, A. I. Levey, G. Li, A. P. Lieberman, K. L. Lunetta, C. G. Lyketsos, D. C. Marson, F. Martinuzzi, D. C. Mash, E. Masliah, W. C. McCormick, S. M. McKus, A. N. McDavid, A. C. McKee, M. Mesulam, B. L. Miller, C. A. Miller, J. W. Miller, J. C. Morris, J. R. Murrell, A. J. Myers, S. O'Bryant, J. M. Olichney, V. S. Pankratz, J. E. Parisi, H. L. Paulson, W. Perry, E. Peskind, A. Pierce, W. W. Poon, H. Potter, J. F. Quinn, A. Raj, M. Raskind, B. Reisberg, C. Reitz, J. M. Ringman, E. D. Roberson, E. Rogaeva, H. J. Rosen, R. N. Rosenberg, M. A. Sager, A. J. Saykin, J. A. Schneider, L. S. Schneider, W. W. Seeley, A. G. Smith, J. A. Sonnen, S. Spina, A. Stern, R. H. Swerdlow, R. E. Tanzi, T. A. Thornton-Wells, J. Q. Trojanowski, J. C. Troncoso, V. M. Van Deerlin, L. J. Van Eldik, H. V. Vinters, J. P. Vonsattel, S. Weintraub, K. A. Welsh-Bohmer, K. C. Wilhelmsen, J. Williamson, T. S. Wingo, R. L. Woltjer, C. B. Wright, C.-E. Yu, L. Yu, F. Garzia, F. Golamaully, G. Septier, S. Engelborghs, R. Vandenberghe, P. P. De Deyn, C. M. Fernandez, Y. A. Benito, H. Thonberg, C. Forsell, L. Lilius, A. Kinhult-Ståhlbom, L. Kilander, R. M. Brundin, L. Conconi, S. Helisalmi, A. M. Koivisto, A. Haapasalo, V. Dermecourt, N. Fievet, O. Hanon, C. Dufouil, A. Brice, K. Ritchie, B. Dubois, J. J. Himali, C. D. Keene, J. A. Tschanz, A. L. Fitzpatrick, W. A. Kukull, M. Norton, T. Aspelund, E. B. Larson, R. Munger, J. I. Rotter, R. B. Lipton, M. J. Bullido, A. Hofman, T. J. Montine, E. Coto, E. Boerwinkle, R. C. Petersen, V. Alvarez, F. Rivadeneira, E. M. Reiman, M. Gallo, C. J. O'Donnell, J. S. Reisch, C. A. Bruni, D. R. Royall, M. Dichgans, M. Sano, D. Galimberti, P. S. George-Hyslop, E. Scarpini, D. W. Tsuang, M. Mancuso, U. Bonuccelli, A. R. Winslow, A. Daniele, C.-K. Wu; GERAD/PERADES, CHARGE, ADGC, EADI, O. Peters, B. Nacmias, M. Riemenschneider, R. Heun, C. Brayne, D. C. Rubinsztein, J. Bras, R. Guerreiro, A. I.-Chalabi, C. E. Shaw, J. Collinge, D. Mann, M. Tsolaki, J. Clarimón, R. Sussams, S. Lovestone, M. C. O'Donovan, M. J. Owen, T. W. Behrens, S. Mead, A. M. Goate, A. G. Uitterlinden, C. Holmes, C. Cruchaga, M. Ingelsson, D. A. Bennett, J. Powell, T. E. Golde, C. Graff, P. L. DeJager, K. Morgan, N. Ertekin-Taner, O. Combarros, B. M. Psaty, P. Passmore, S. G. Younkin, C. Berr, V. Gudnason, D. Rujescu, D. W. Dickson, J.-F. Dartigues, A. L. DeStefano, S. Ortega-Cubero, H. Hakonarson, D. Campion, M. Boada, J. K. Kauwe, L. A. Farrer, C. Van Broeckhoven, M. A. Ikram, L. Jones, J. L. Haines, C. Tzourio, L. J. Launer, V. Escott-Price, R. Mayeux, J.-F. Deleuze, N. Amin, P. A. Holmans, M. A. Pericak-Vance, P. Amouyel, C. M. van Duijn, A. Ramirez, L.-S. Wang, J.-C. Lambert, S. Seshadri, J. Williams, G. D. Schellenberg. Rare coding variants in *PLCG2*, *AB13*, and *TREM2* implicate microglial-mediated innate immunity in Alzheimer's disease. *Nat. Genet.* **49**, 1373–1384 (2017).
11. S. J. van der Lee, O. J. Conway, I. Jansen, M. M. Carrasquillo, L. Kleiheidam, E. van den Akker, I. Hernández, K. R. van Eijk, K. Chen, A. Chen, A. Zettergren, T. F. M. Andlauer, M. Diez-Fairen, J. Simon-Sanchez, A. Lleó, H. Zetterberg, M. Nygaard, C. Blauwendraat, J. E. Savage, J. Mengel-From, S. Moreno-Grau, M. Wagner, J. Fortea, M. J. Keogh, K. Blennow, I. Skoog, M. A. Friesse, O. Pletnikova, M. Zulaica, C. Lage, I. de Rojas, S. Riedel-Heller, I. Illán-Gala, W. Wei, B. Jeune, A. Orellana, F. T. Bergh, X. Wang, M. Hulsman, N. Beker, N. Tesi, C. M. Morris, B. Indakoetxea, L. E. Collij, M. Scherer, E. Morenas-Rodriguez, J. W. Ironside, B. N. M. van Berckel, D. Alcolea, H. Wiendl, S. L. Strickland, P. Pastor, E. R. Rodriguez; DESGESCO (Dementia Genetics Spanish Consortium), EADB (Alzheimer Disease European DNA biobank); EADB (Alzheimer Disease European DNA biobank); IFGC (International FTD-Genomics Consortium), IPDGC (The International Parkinson Disease Genomics Consortium); IPDGC (The International Parkinson Disease Genomics Consortium); RiMod-FTD (Risk and Modifying factors in Fronto-Temporal Dementia); Netherlands Brain Bank (NBB); B. F. Boeve, R. C. Petersen, T. J. Ferren, J. A. van Gerpen, M. J. T. Reinders, R. J. Ulitti, L. Tárraga, W. Maier, O. Dols-Icardo, A. Kawalia, M. C. Dalmaso, M. Boada, U. K. Zettl, N. M. van Schoor, M. Beekman, M. Allen, E. Masliah, A. L. de Munain, A. Pantelyat, Z. K. Wszolek, O. A. Ross, D. W. Dickson, N. R. Graff-Radford, D. Knopman, R. Rademakers, A. W. Lemstra, Y. A. L. Pijnenburg, P. Scheltens, T. Gasser, P. F. Chinnery, B. Hemmer, M. A. Huisman, J. Troncoso, F. Moreno, E. A. Nohr, T. I. A. Sørensen, P. Heutink, P. Sánchez-Juan, D. Posthuma; GIFT (Genetic Investigation in Frontotemporal Dementia and Alzheimer's Disease) Study Group, J. Clarimón, K. Christensen, N. Ertekin-Taner, S. W. Scholz, A. Ramirez, A. Ruiz, E. Slagboom, W. M. van der Flier, H. Holstege, A nonsynonymous mutation in *PLCG2* reduces the risk of Alzheimer's disease, dementia with Lewy bodies and frontotemporal dementia, and increases the likelihood of longevity. *Acta Neuropathol.* **138**, 237–250 (2019).
12. L. O. Essen, O. Perisic, R. Cheung, M. Katan, R. L. Williams, Crystal structure of a mammalian phosphoinositide-specific phospholipase C delta. *Nature* **380**, 595–602 (1996).
13. M. R. Jczyk, J. T. Snyder, S. Gershberg, D. K. Worthylake, T. K. Harden, J. Sondek, Crystal structure of Rac1 bound to its effector phospholipase C-β2. *Nat. Struct. Mol. Biol.* **13**, 1135–1140 (2006).
14. G. L. Waldo, T. K. Ricks, S. N. Hicks, M. L. Cheever, T. Kawano, K. Tsuboi, X. Wang, C. Montell, T. Kozasa, J. Sondek, T. K. Harden, Kinetic scaffolding mediated by a phospholipase C-beta and Gq signaling complex. *Science* **330**, 974–980 (2010).
15. A. M. Lyon, V. M. Tesmer, V. D. Dhamsania, D. M. Thal, J. Gutierrez, S. Chowdhury, K. C. Suddala, J. K. Northup, J. J. G. Tesmer, An autoinhibitory helix in the C-terminal region of phospholipase C-β mediates Gαq activation. *Nat. Struct. Mol. Biol.* **18**, 999–1005 (2011).
16. A. M. Lyon, J. A. Begley, T. D. Manett, J. J. G. Tesmer, Molecular mechanisms of phospholipase C β3 autoinhibition. *Structure* **22**, 1844–1854 (2014).
17. A. M. Lyon, S. Dutta, C. A. Boguth, G. Skiniotis, J. J. Tesmer, Full-length Gαq–phospholipase C-β3 structure reveals interfaces of the C-terminal coiled-coil domain. *Nat. Struct. Mol. Biol.* **20**, 355–362 (2013).
18. N. Hajicek, N. C. Keith, E. Siraliev-Perez, B. R. S. Temple, W. Huang, Q. Zhang, T. K. Harden, J. Sondek, Structural basis for the activation of PLC-γ isozymes by phosphorylation and cancer-associated mutations. *eLife* **8**, e51700 (2019).
19. Y. Liu, T. D. Bunney, S. Khosa, K. Macé, K. Beckenbauer, T. Askwith, S. Maslen, C. Stubbs, T. M. de Oliveira, K. Sader, M. Skehel, A.-C. Gavin, C. Phillips, M. Katan, Structural insights and activating mutations in diverse pathologies define mechanisms of deregulation for phospholipase C gamma enzymes. *Elife* **9**, 102607 (2020).
20. N. Y. Rugema, E. E. Garland-Kuntz, M. Sieng, K. Muralidharan, M. M. van Camp, H. O'Neill, W. Mbongo, A. F. Selvia, A. T. Marti, A. Everly, E. McKenzie, A. M. Lyon, Structure of phospholipase Cε reveals an integrated RA1 domain and previously unidentified regulatory elements. *Commun. Biol.* **3**, 445 (2020).
21. T. H. Charpentier, G. L. Waldo, M. O. Barrett, W. Huang, Q. Zhang, T. K. Harden, J. Sondek, Membrane-induced allosteric control of phospholipase C-β isozymes. *J. Biol. Chem.* **289**, 29545–29551 (2014).
22. A. Arduin, P. R. Gaffney, O. Ces, Regulation of PLCβ2 by the electrostatic and mechanical properties of lipid bilayers. *Sci. Rep.* **5**, 12628 (2015).
23. B. N. Hudson, S. H. Hyun, D. H. Thompson, A. M. Lyon, Phospholipase Cβ3 membrane adsorption and activation are regulated by its C-terminal domains and phosphatidylinositol 4,5-bisphosphate. *Biochemistry* **56**, 5604–5614 (2017).
24. B. N. Hudson, R. E. Jessup, K. K. Prahalad, A. M. Lyon, Gαq and the phospholipase Cβ3 XY-linker regulate adsorption and activity on compressed lipid monolayers. *Biochemistry* **58**, 3454–3467 (2019).
25. I. Fisher, M. Jenkins, G. Tall, J. Burke, A. Smrcka, Activation of phospholipase C β by Gβγ and Gαq involves c-terminal rearrangement to release autoinhibition. *Structure* **28**, 810–819.e5 (2020).
26. M. Falasca, S. K. Logan, V. P. Lehto, G. Baccante, M. A. Lemmon, J. Schlessinger, Activation of phospholipase Cgamma by PI 3-kinase-induced PH domain-mediated membrane targeting. *EMBO J.* **17**, 414–422 (1998).
27. M. Nishida, K. Sugimoto, Y. Hara, E. Mori, T. Morii, T. Kurosaki, Y. Mori, Amplification of receptor signalling by Ca²⁺ entry-mediated translocation and activation of PLCγ2 in B lymphocytes. *EMBO J.* **22**, 4677–4688 (2003).
28. S. J. Marrink, V. Corradi, P. C. T. Souza, H. I. Ingólfsson, D. P. Tieleman, M. S. P. Sansom, Computational modeling of realistic cell membranes. *Chem. Rev.* **119**, 6184–6226 (2019).
29. M. Moqadam, T. Tubiana, E. Moutoussamy, N. Reuter, Membrane models for molecular simulations of peripheral membrane proteins. *Adv. Phys. X* **6**, 1932589 (2021).
30. A. C. Kalli, M. S. P. Sansom, Interactions of peripheral proteins with model membranes as viewed by molecular dynamics simulations. *Biochem. Soc. Trans.* **42**, 1418–1424 (2014).
31. F. Naughton, "Interactions of peripheral membrane proteins with phosphatidylinositol lipids: Insights from molecular dynamics simulations," thesis, University of Oxford (2018).
32. Q. N. Van, C. A. López, M. Tonelli, T. Taylor, B. Niu, C. B. Stanley, D. Bhowmik, T. H. Tran, P. H. Frank, S. Messing, P. Alexander, D. Scott, X. Ye, M. Drew, O. Chertov, M. Lösche, A. Ramanathan, M. L. Gross, N. W. Hengartner, W. M. Westler, J. L. Markley, D. K. Simanshu, D. V. Nissley, W. K. Gillette, D. Esposito, F. McCormick, S. Gnanakaran, F. Heinrich, A. G. Stephen, Uncovering a membrane-distal conformation of KRAS available to recruit RAF to the plasma membrane. *Proc. Natl. Acad. Sci. U.S.A.* **117**, 24258–24268 (2020).
33. S. Ahmad, C. H. Strunk, S. N. Schott-Verdugo, K.-E. Jaeger, F. Kovacic, H. Gohlke, Substrate access mechanism in a novel membrane-bound phospholipase A of *Pseudomonas aeruginosa* concordant with specificity and regioselectivity. *J. Chem. Inf. Model.* **61**, 5626–5643 (2021).
34. K. I. P. Le Huray, H. Wang, F. Sobott, A. C. Kalli, Systematic simulation of the interactions of Pleckstrin homology domains with membranes. *bioRxiv* 2021.12.16.472954 (2021).
35. E. Yamamoto, J. Domański, F. B. Naughton, R. B. Best, A. C. Kalli, P. J. Stansfeld, M. S. P. Sansom, Multiple lipid binding sites determine the affinity of PH domains for phosphoinositide-containing membranes. *Sci. Adv.* **6**, eaay5736 (2020).
36. V. M. Patel, C. E. Flanagan, M. Martins, C. L. Jones, R. M. Butler, W. J. Woollard, F. S. Bakr, A. Yoxall, N. Begum, M. Katan, S. J. Whittaker, T. J. Mitchell, Frequent and Persistent *PLCG1* mutations in sézary cells directly enhance PLCγ1 activity and stimulate NFκB, AP-1, and NFAT signaling. *J. Invest. Dermatol.* **140**, 380–389.e4 (2020).
37. A. Gresset, S. N. Hicks, T. K. Harden, J. Sondek, Mechanism of Phosphorylation-induced Activation of Phospholipase C-γ Isozymes. *J. Biol. Chem.* **285**, 35836–35847 (2010).
38. K. L. Everett, A. Buehler, T. D. Bunney, A. Margineanu, R. W. Baxendale, P. Vatter, M. Retlich, C. Walliser, H. B. Manning, M. A. A. Neil, C. Dunsby, P. M. W. French, P. Gierschik, M. Katan, Membrane environment exerts an important influence on rac-mediated activation of phospholipase Cγ2. *Mol. Cell. Biol.* **31**, 1240–1251 (2011).
39. T. D. Bunney, D. Esposito, C. Mas-Droux, E. Lamber, R. W. Baxendale, M. Martins, A. Cole, D. Svergun, P. C. Driscoll, M. Katan, Structural and functional integration of the PLCγ

- interaction domains critical for regulatory mechanisms and signaling deregulation. *Structure* **20**, 2062–2075 (2012).
40. M. V. Ellis, S. R. James, O. Perisic, C. P. Downes, R. L. Williams, M. Katan, Catalytic domain of phosphoinositide-specific phospholipase C (PLC). *J. Biol. Chem.* **273**, 11650–11659 (1998).
 41. K. I. Everett, T. D. Bunney, Y. Yoon, F. Rodrigues-Lima, R. Harris, P. C. Driscoll, K. Abe, H. Fuchs, M. H. de Angelis, P. Yu, W. Cho, M. Katan, Characterization of phospholipase C γ enzymes with gain-of-function mutations. *J. Biol. Chem.* **284**, 23083–23093 (2009).
 42. M. Javanainen, H. Martinez-Seara, I. Vattulainen, Excessive aggregation of membrane proteins in the Martini model. *PLoS ONE* **12**, e0187936 (2017).
 43. J. W. Lomasney, H.-F. Cheng, M. Kobayashi, K. King, Structural basis for calcium and phosphatidylserine regulation of phospholipase C δ 1. *Biochemistry* **51**, 2246–2257 (2012).
 44. B. Ananthanarayanan, S. Das, S. G. Rhee, D. Murray, W. Cho, Membrane targeting of C2 domains of phospholipase C- δ isoforms*. *J. Biol. Chem.* **277**, 3568–3575 (2002).
 45. J. Cai, S. Guo, J. W. Lomasney, M. F. Roberts, Ca $^{2+}$ -independent binding of anionic phospholipids by phospholipase C δ 1 EF-hand domain. *J. Biol. Chem.* **288**, 37277–37288 (2013).
 46. M. Nomikos, J. R. Sanders, D. Parthimos, L. Buntwal, B. L. Calver, P. Stamatiadis, A. Smith, M. Clue, Z. Sideratou, K. Swann, F. A. Lai, Essential role of the EF-hand domain in targeting sperm phospholipase C ζ to membrane phosphatidylinositol 4,5-bisphosphate (PIP2). *J. Biol. Chem.* **290**, 29519–29530 (2015).
 47. D. Vallois, M. P. D. Dobay, R. D. Morin, F. Lemonnier, E. Missiaglia, M. Juillard, J. Iwaszkiewicz, V. Fataccioli, B. Bisig, A. Roberti, J. Grewal, J. Bruneau, B. Fabiani, A. Martin, C. Bonnet, O. Michielin, J.-P. Jais, M. Figeac, O. A. Bernard, M. Delorenzi, C. Haioun, O. Tournilhac, M. Thome, R. D. Gascoyne, P. Gaulard, L. de Leval, Activating mutations in genes related to TCR signaling in angioimmunoblastic and other follicular helper T-cell-derived lymphomas. *Blood* **128**, 1490–1502 (2016).
 48. D. F. J. Ceccarelli, I. M. Blasutig, M. Goudreaux, Z. Li, J. Ruston, T. Pawson, F. Sicheri, Non-canonical interaction of phosphoinositides with pleckstrin homology domains of Tiam1 and ArhGAP9. *J. Biol. Chem.* **282**, 13864–13874 (2007).
 49. N. Hajicek, T. H. Charpentier, J. R. Rush, T. K. Harden, J. Sondck, Autoinhibition and phosphorylation-induced activation of phospholipase C- γ isozymes. *Biochemistry* **52**, 4810–4819 (2013).
 50. E. M. Ross, G α q and phospholipase C- β : Turn on, turn off, and do it fast. *Sci. Signal.* **4**, pe5 (2011).
 51. K. Muralidharan, M. M. Van Camp, A. M. Lyon, Structure and regulation of phospholipase C β and ϵ at the membrane. *Chem. Phys. Lipids* **235**, 105050 (2021).
 52. B. N. Hudson, R. E. Jessup, K. K. Prahalad, A. M. Lyon, G α q and the phospholipase C β 3 XY-linker regulate adsorption and activity on compressed lipid monolayers. *Biochemistry* **58**, 3454–3467 (2019).
 53. J. Lowe, R. E. Joseph, A. H. Andreotti, Conformational switches that control the TEC kinase – PLC γ signaling axis. *J. Struct. Biol.* **X 6**, 100061 (2022).
 54. R. E. Joseph, J. Lowe, D. B. Fulton, J. R. Engen, T. E. Wales, A. H. Andreotti, The conformational state of the BTK substrate PLC γ contributes to ibrutinib resistance. *J. Mol. Biol.* **434**, 167422 (2022).
 55. J. Wada, U. Rathnayake, L. M. Jenkins, A. Singh, M. Mohammadi, E. Appella, P. A. Randazzo, L. E. Samelson, In vitro reconstitution reveals cooperative mechanisms of adapter protein-mediated activation of phospholipase C- γ 1 in T cells. *J. Biol. Chem.* **298**, 101680 (2022).
 56. G. Hedger, M. S. P. Sansom, Lipid interaction sites on channels, transporters and receptors: Recent insights from molecular dynamics simulations. *Biochim. Biophys. Acta - Biomembranes* **1858**, 2390–2400 (2016).
 57. W. Kabsch, Integration, scaling, space-group assignment and post-refinement. *Acta Crystallogr. D Biol. Crystallogr.* **66**, 133–144 (2010).
 58. A. Vagin, A. Teplyakov, Molecular replacement with MOLREP. *Acta Crystallogr. D Biol. Crystallogr.* **66**, 22–25 (2010).
 59. P. D. Adams, P. V. Afonine, G. Bunkóczi, V. B. Chen, I. W. Davis, N. Echols, J. J. Headd, L. W. Hung, G. J. Kapral, R. W. Grosse-Kunstleve, A. J. McCoy, N. W. Moriarty, R. Oeffner, R. J. Read, D. C. Richardson, J. S. Richardson, T. C. Terwilliger, P. H. Zwart, PHENIX: A comprehensive Python-based system for macromolecular structure solution. *Acta Crystallogr. D Biol. Crystallogr.* **66**, 213–221 (2010).
 60. P. Emsley, B. Lohkamp, W. G. Scott, K. Cowtan, Features and development of Coot. *Acta Crystallogr. D Biol. Crystallogr.* **66**, 486–501 (2010).
 61. S. J. Marrink, H. J. Risselada, S. Yefimov, D. P. Tieleman, A. H. de Vries, The MARTINI force field: Coarse grained model for biomolecular simulations. *J. Phys. Chem. B* **111**, 7812–7824 (2007).
 62. M. J. Abraham, R. Murtola, R. Schulz, S. Páll, J. C. Smith, B. Hess, E. Lindahl, GROMACS: High performance molecular simulations through multi-level parallelism from laptops to supercomputers. *SoftwareX* **1–2**, 19–25 (2015).
 63. A. Fiser, A. Sali, MODELLER: Generation and refinement of homology-based protein structure models. *Methods Enzymol.* **374**, 461–491 (2003).
 64. D. H. De Jong, G. Singh, W. F. D. D. Bennett, C. Arnarez, T. A. Wassenaar, L. V. Schäfer, X. Periole, D. P. Tieleman, S. J. Marrink, W. F. Drew Bennett, C. Arnarez, T. A. Wassenaar, L. V. Schäfer, X. Periole, D. Peter, S. J. Marrink, Improved parameters for the martini coarse-grained protein force field. *J. Chem. Theory Comput.* **9**, 687–697 (2013).
 65. T. A. Wassenaar, H. I. Inglfsson, R. A. Bckmann, D. P. Tieleman, S. J. Marrink, Computational lipidomics with *insane*: A versatile tool for generating custom membranes for molecular simulations. *J. Chem. Theory Comput.* **11**, 2144–2155 (2015).
 66. G. Bussi, D. Donadio, M. Parrinello, Canonical sampling through velocity rescaling. *J. Chem. Phys.* **126**, 014101 (2007).
 67. M. Parrinello, A. Rahman, Polymorphic transitions in single crystals: A new molecular dynamics method. *J. Appl. Phys.* **52**, 7182–7190 (1981).
 68. T. A. Wassenaar, K. Pluhackova, R. A. Böckmann, S. J. Marrink, D. P. Tieleman, Going backward: A flexible geometric approach to reverse transformation from coarse grained to atomistic models. *J. Chem. Theory Comput.* **10**, 676–690 (2014).
 69. R. B. Best, X. Zhu, J. Shim, P. E. M. Lopes, J. Mittal, M. Feig, A. D. MacKerell, Optimization of the additive CHARMM all-atom protein force field targeting improved sampling of the backbone ϕ , ψ and side-chain χ 1 and χ 2 dihedral angles. *J. Chem. Theory Comput.* **8**, 3257–3273 (2012).
 70. S. Jo, T. Kim, V. G. Iyer, W. Im, CHARMM-GUI: A web-based graphical user interface for CHARMM. *J. Comput. Chem.* **29**, 1859–1865 (2008).
 71. D. R. Slochow, P. J. Huwe, R. Radhakrishnan, P. A. Janney, Quantum and all-atom molecular dynamics simulations of protonation and divalent ion binding to phosphatidylinositol 4,5-bisphosphate (PIP2). *J. Phys. Chem. B* **117**, 8322–8329 (2013).
 72. W. Humphrey, A. Dalke, K. Schulten, VMD: Visual molecular dynamics. *J. Mol. Graph.* **14**, 33–38 (1996).
 73. R. B. Russell, G. J. Barton, Multiple protein sequence alignment from tertiary structure comparison: Assignment of global and residue confidence levels. *Proteins* **14**, 309–323 (1992).
 74. A. M. Waterhouse, J. B. Procter, D. M. A. Martin, M. Clamp, G. J. Barton, Jalview version 2—A multiple sequence alignment editor and analysis workbench. *Bioinformatics* **25**, 1189–1191 (2009).

Acknowledgments: MD simulations were undertaken on ARC3 and ARC4, part of the High-Performance Computing facilities at the University of Leeds, United Kingdom. We are grateful to G. Gong for help with the liposome binding assay and to M. Edwards for help with cell culture. Protein crystallography data collection was performed on beamline ID32-1 at the European Synchrotron Radiation Facility (ESRF), Grenoble, France. We are grateful to A. Popov at the ESRF for providing assistance in using the beamline. We would like to acknowledge F. Sobott for useful discussions. **Funding:** Biotechnology and Biological Sciences Research Council grant BB/M011151/1 (K.I.P.L.H. and A.C.K.), The Fidelity Bermuda Foundation award number 180348 (T.D.B. and M.K.), The UCL Therapeutic Acceleration Support (TAS) Fund award number 560655 (T.D.B. and M.K.), and Wellcome Trust Multi-User Equipment grant 221543/Z/20/Z (N.P.). Research in A.C.K.'s group is also supported by the British Heart Foundation (PG/21/10515). **Author contributions:** Conceptualization: A.C.K., K.I.P.L.H., M.K., and T.D.B. Methodology: A.C.K., K.I.P.L.H., M.K., N.P., and T.D.B. MD simulation and analysis: K.I.P.L.H. Protein production and biochemical assays: T.D.B. Protein crystallography: N.P. Visualization: K.I.P.L.H., M.K., and T.D.B. Supervision: A.C.K., M.K., and T.D.B. Writing—original draft: K.I.P.L.H., M.K., and T.D.B. Writing—review and editing: A.C.K., K.I.P.L.H., M.K., N.P., and T.D.B. **Competing interests:** The authors declare that they have no competing interests. **Data and materials availability:** All data needed to evaluate the conclusions in the paper are present in the paper and/or the Supplementary Materials. The information for crystal structure is deposited with the PDB ID: 7Z3J. A repository of simulation data is available at <https://doi.org/10.5518/1133>.

Submitted 10 March 2022

Accepted 6 May 2022

Published 24 June 2022

10.1126/sciadv.abp9688

Characterization of the membrane interactions of phospholipase C# reveals key features of the active enzyme

Kyle I. P. Le Huray, Tom D. Bunney, Nikos Pinotsis, Antreas C. Kalli, and Matilda Katan

Sci. Adv., **8** (25), eabp9688.
DOI: 10.1126/sciadv.abp9688

View the article online

<https://www.science.org/doi/10.1126/sciadv.abp9688>

Permissions

<https://www.science.org/help/reprints-and-permissions>

Use of this article is subject to the [Terms of service](#)